CrossMark

JM PAPERS

Geometric-control formulation and averaging analysis of the unsteady aerodynamics of a wing with oscillatory controls

Haithem E. Taha[1,†], **Laura Pla Olea**[1], **Nabil Khalifa**[1], **Cody Gonzalez**[1] **and Amir S. Rezaei**[1]

[1]Mechanical and Aerospace Engineering, University of California, Irvine, CA 92697, USA

Differential-geometric-control theory represents a mathematically elegant combination of differential geometry and control theory. Practically, it allows exploitation of nonlinear interactions between various inputs for the generation of forces in non-intuitive directions. Since its early developments in the 1970s, the geometric-control theory has not been duly exploited in the area of fluid mechanics. In this paper, we show the potential of geometric-control theory in the analysis of fluid flows, exemplifying it as a heuristic analysis tool for discovery of symmetry-breaking and unconventional force-generation mechanisms. In particular, we formulate the wing unsteady aerodynamics problem in a geometric-control framework. To achieve this goal, we develop a reduced-order model for the unsteady flow over a pitching–plunging wing that is (i) rich enough to capture the main physical aspects (e.g. nonlinearity of the flow dynamics at large angles of attack and high frequencies) and (ii) efficient and compact enough to be amenable to the analytic tools of geometric nonlinear control theory. We then combine tools from geometric-control theory and averaging to analyse the developed reduced-order dynamical model, which reveals regimes for lift and thrust enhancement mechanisms. The unsteady Reynolds-averaged Navier–Stokes equations are simulated to validate the theoretical findings and scrutinize the underlying physics behind these enhancement mechanisms.

Key words: control theory, general fluid mechanics, vortex interactions

1. Introduction

Unsteady aerodynamics of airfoils subject to oscillatory inputs/controls is a classical problem in aerodynamics whose history can be traced to Theodorsen (1935). More recent efforts are concerned with oscillations at large angles of attack, high frequencies

and/or with large amplitudes (Rival & Tropea 2010; Baik *et al.* 2012; Cleaver, Wang & Gursul 2012; Wang & Eldredge 2013; Hemati, Eldredge & Speyer 2014; Ramesh *et al.* 2014; Taha, Hajj & Beran 2014; Choi, Colonius & Williams 2015; Chiereghin, Cleaver & Gursul 2019; Gupta & Ansell 2019). In these studies, the effect of flow nonlinearities is considerable and sometimes leads to interesting unconventional force-generation mechanisms via symmetry breaking. In the literature of mathematical control theory, differential-geometric control has been a very useful tool in analysing nonlinear dynamical systems; it allows engineers to exploit nonlinear interactions to generate forces in unactuated directions (Crouch 1984; Murray, Li & Sastry 1994; Leonard & Krishnaprasad 1995; Walsh & Sastry 1995; Morgansen *et al.* 2001; Bullo & Lewis 2004; Taha, Woolsey & Hajj 2015*b*). Hence, the formulation of unsteady aerodynamics in a differential-geometric-control framework seems natural, in addition to being mathematically elegant – this is the overarching goal of this paper: to formulate the unsteady aerodynamics of an airfoil with oscillatory inputs in a geometric-control framework. This formulation may help deepen our understanding of the flow nonlinear mechanisms and provide a clue as to how we can exploit them to achieve performance that cannot be achieved in a linear, small-angle-of-attack environment. However, this formulation requires special reduced-order modelling to be amenable to geometric-control mathematical tools (it is a model-based theory).

The main contribution and focus of this paper is threefold. First, we aim to develop a physics-based reduced-order model (ROM) of the aerodynamic loads over a pitching–plunging wing that captures essential unsteady, nonlinear effects at high angles of attack and high frequencies, yet is represented in a compact form (state space form) amenable to nonlinear systems theory. Second, we apply differential-geometric control and averaging to the developed ROM as a heuristic approach to discover unconventional lift and thrust enhancement mechanisms at high angles of attack. Third, we perform higher-fidelity computational simulations of the unsteady Reynolds-averaged Navier–Stokes (URANS) equations to study the flow physics underlying these lift and thrust enhancement mechanisms.

As may be expected from the above goals, the paper includes tools and language developed in two separate fields: unsteady aerodynamics and nonlinear control theory. It is our hope that we bridge a gap between these two disciplines and provide an example where consolidation between the two is worth pursuing.

1.1. *Reduced-order modelling of unsteady aerodynamics*

Unsteady aerodynamics of oscillatory wings has a long-standing history since Wagner's and Theodorsen's seminal efforts (Wagner 1925; Theodorsen 1935); its vast literature (extending over a century) may not be fathomable in a single article. The pioneering modelling efforts by Wagner (1925), Theodorsen (1935), Von Kármán & Sears (1938) among others (Küssner 1929; Garrick 1938; Schwarz 1940; Sears 1941; Loewy 1957) were mainly based on potential flow. They resulted in infinite-dimensional responses for the unsteady lift dynamics, e.g. step response (Wagner 1925) and frequency response (Theodorsen 1935). That is, in a dynamical-systems narrative, the lift transfer function has infinitely many poles (Peters 2008). The need for more compact representations of these models for structural and/or dynamic coupling (to assess aeroelastic and/or flight dynamic stability problems) has led to a number of finite-dimensional approximations (Jones 1938, 1945; Vepa 1976; Leishman & Nguyen 1990; Peters, Karunamoorthy & Cao 1995;

Peters 2008). However, all these models are linear, allowing only small disturbances to the mean flow.

On the other hand, the available mathematical models for the analysis of unsteady nonlinear aerodynamics at high angles of attack are not as abundant as the linear ones. There are some *ad hoc* models, such as the Beddoes–Leishman dynamic stall model (Leishman & Beddoes 1989; Leishman & Crouse 1989) and the Goman–Khrabrov model (Goman & Khrabrov 1994). With the increased research interests in bio-inspired flight, more vivid research activities on the unsteady aerodynamics at high angles of attack and low Reynolds numbers have occurred. In particular, several models have been developed to capture the unsteady, nonlinear effects of the leading-edge vortex on lift dynamics (Minotti 2002; Jones 2003; Yongliang, Binggang & Huiyang 2003; Pullin & Wang 2004; Ansari, Żbikowski & Knowles 2006; Wang & Eldredge 2013; Hemati *et al.* 2014; Ramesh *et al.* 2014; Taha *et al.* 2014; Yan, Taha & Hajj 2014; Li & Wu 2015). However, almost all of these models are not amenable to nonlinear systems theory analysis; most of them rely on discrete vortex methods whose size grows with time.

More recently, there have been formal techniques to develop reduced-order models using dynamic mode decomposition (Rowley *et al.* 2009; Abraham, De La Torre & Murphey 2017; Huang & Vaidya 2018) and sparse identification (Brunton, Proctor & Kutz 2016*b*). The current approach has a similar spirit to these techniques, however, it proposes a specific model structure that is particularly suitable for the oscillating airfoil problem – such a structure is inspired from the classical theory of unsteady aerodynamics (Von Kármán & Sears 1938). In other words, the proposed model provides an extension of the classical theory to high angles of attack. That is, the unique aspect of the developed model lies in (i) capturing unsteady nonlinear characteristics at high angles of attack, and (ii) its convenience for the application of nonlinear systems analysis tools, in particular geometric-control theory and averaging.

1.2. *Effect of airfoil oscillations on lift and thrust enhancement: symmetry breaking*

Earlier interests in studying the dynamic stall phenomenon have triggered numerous research efforts on the subject (e.g. McCroskey *et al.* 1982; Carr 1988; Ekaterinaris & Platzer 1998; Lee & Gerontakos 2004; Andro & Jacquin 2009; Rival & Tropea 2010; Gupta & Ansell 2019); they studied the phenomenon of unsteady lift increase beyond the static values when executing a dynamic manoeuvre near stall. More recent reports focused more on the unsteady flow physics underlying such lift enhancement (Rival & Tropea 2010; Cleaver *et al.* 2011, 2012; Baik *et al.* 2012; Cleaver, Wang & Gursul 2013; Choi *et al.* 2015; Chiereghin *et al.* 2019; Gupta & Ansell 2019).

In general, when applying an oscillatory flow control, the lift and thrust responses will be oscillatory; their mean values may be expected to match the steady values in the absence of flow-control oscillations. However, the cycle-averaged forces may be different from the steady values, indicating a symmetry breaking. There are classical examples such as the well-known thrust symmetry breaking due to pitching or plunging airfoils at high enough frequency (Garrick 1937; Sedov 1980; Lighthill 1975; Rozhdestvensky & Ryzhov 2003). In addition, there are less intuitive, more interesting symmetry breaking mechanisms. For example, it may be expected that symmetric plunging in a quiescent fluid will not generate net forces. However, Vandenberghe, Zhang & Childress (2004) and Alben & Shelley (2005) showed a symmetry breaking if oscillation takes place at a high enough frequency; the free foil started to move forward, indicating a net thrust force.

Similarly, it may be expected that symmetric plunging (or pitching) oscillations (even in a moving stream) do not lead to a net-lift force: an extra lift is gained during the

downstroke and an equal amount of lift is lost during the upstroke, leading to a zero net lift beyond the steady value corresponding to the mean angle of attack. However, it is envisaged that symmetry breaking might occur beyond a certain threshold of oscillation frequency that would lead to a non-zero, net-lift force. Many efforts have been made to study such a symmetry-breaking mechanism using extensive high-fidelity simulations and experiments (Rival & Tropea 2010; Baik *et al.* 2012; Gursul, Cleaver & Wang 2014; Panah & Buchholz 2014; Rival *et al.* 2014); but no theoretical efforts have been made in this regard, simply because of the lack of a rich enough ROM and appropriate analysis tools. In this paper, we show how the application of combined geometric-control-averaging analysis tools to the developed ROM can help identifying the key parameters enabling such a symmetry-breaking mechanism via a systematic analysis. We then distil the underlying flow physics to better understand the fluid mechanics principles behind such symmetry breaking, which leads to lift and thrust enhancement.

1.3. *Differential-geometric mechanics and control and its application to fluid problems*

The mathematical theory of differential-geometric control is concerned with dynamical systems evolving on curvy spaces, called manifolds. This covers a fairly large class of mechanical systems (e.g. all systems having rotational degrees of freedom). Adopting this geometric view for these dynamical systems requires an appropriate mathematical tool to perform calculus on curvy spaces: differential geometry. One can loosely say that geometric-control theory is the intersection of differential geometry and control theory of dynamical systems. Aside from the mathematical elegance of differential geometric control, it can be quite useful to control engineers in at least the following three ways (i) it allows motion generation in unactuated directions, by exploiting nonlinear interactions between two or more inputs; (ii) it allows unconventional force generation via symmetry breaking due to a fast, oscillatory control; and (iii) unconventional stabilization due to high-frequency periodic forcing: vibrational control theory.

Since its early developments in the 1970s and 1980s by Roger Brockett (1972; 1976; 1982; 1983) and Hector Sussmann (1972; 1973; 1987) among others, the geometric-control theory has been used to reveal interesting nonlinear dynamical behaviours and motion planning algorithms for spacecraft (rigid body) attitude dynamics and control (Crouch 1984; Leonard & Krishnaprasad 1995; Walsh & Sastry 1995), robotics (Murray *et al.* 1994; Morgansen *et al.* 2001; Vela, Morgansen & Burdick 2002; Woolsey & Leonard 2002; Bullo & Lewis 2004) and more recently bio-inspired flight (Taha *et al.* 2015*b*; Tahmasian & Woolsey 2017; Mir *et al.* 2018; Hassan & Taha 2019). However, it has not been aptly applied to fluid mechanic systems.

Here, it may be prudent to distinguish between a geometric-mechanics formulation and a geometric-control one. While both utilize a differential-geometric language to describe a dynamical system, they are fundamentally different. The former is as old as the work of Jacobi in the 19th century on geometrization of mechanics (Dugas 1988, p. 407), which flourished and matured after the development of Riemannian geometry, to culminate in Einstein's general relativity. In this formulation, the trajectories of a dynamical system are seen as straight lines (geodesics) in some curved space (manifold); e.g. Einstein's general relativity implies that the trajectories of a planetary orbit are geodesics in the curved four-dimensional space–time world whose curvature is determined by gravity. Similarly, there have been several efforts in formulating fluid flows in a geometric-mechanics framework. For example, Arnold showed that the trajectories of ideal (inviscid incompressible) fluid particles are geodesics in the curved space of

volume-preserving diffeomorphisms (Arnold 1966*a*,*b*, 1969). The efforts of Marsden & Weinstein (1983), Holm, Marsden & Ratiu (1998) and Bloch *et al.* (2000) are also worth mentioning in this regard. Most of these efforts are nicely summarized in Arnold's (2013) and Kambe's (2009) books. With a similar spirit, there are several efforts made to construct a Hamiltonian structure for the dynamics of point vortices interacting with a rigid body in an ideal flow in the two-dimensional case of zero circulation around the body (Shashikanth *et al.* 2002; Shashikanth 2005), arbitrary circulation around the body (Borisov, Mamaev & Ramodanov 2003, 2007), the three-dimensional case (Shashikanth *et al.* 2008, 2010; Dritschel & Boatto 2015) and the case of unsteady (time-varying) point vortices (Hussein *et al.* 2018).

On the other hand, the differential-geometric-control formulation of dynamical systems is relatively recent in comparison with geometric mechanics. It started in the 1960s with Hermann's seminal efforts (Hermann 1962, 1963). The focus of this formulation is on the control of general dynamical systems; no Hamiltonian/Lagrangian structure is required, in contrast to the geometric-mechanics formulation. Also, the objective is to perform control theoretic analysis such as stability, controllability, observability, motion planning, etc. While there have been several efforts made for a geometric-mechanics formulation of fluid flows (particularly ideal fluids), as discussed above, there have been no efforts made for a geometric-control formulation. Perhaps the closest efforts are those of Kelly, Kanso and Tallapragada among others (Kelly & Murray 2000; Kanso *et al.* 2005; Kelly & Hukkeri 2006; Tallapragada & Kelly 2017; Buzhardt, Fedonyuk & Tallapragada 2018). However, these interesting efforts were mostly concerned with geometric-control aspects of locomotion; i.e. interaction of a swimming body with the surrounding flow to propel itself. So, the main dynamics is that of the body; and simplistic models were used for the flow dynamics. For example, the early trials by Kelly & Murray (2000) and Kelly & Hukkeri (2006) completely ignored the flow dynamics and focused on the body motion subject to an idealized flow control input: quasi-steady vortex strength and location (Kelly & Murray 2000), and quasi-steady lift force normal to the instantaneous velocity of the body (Kelly & Hukkeri 2006). Using a different formulation, Kanso *et al.* (2005) assumed an ideal flow with zero net circulation around the body (i.e. no vortex shedding). So, they only accounted for added-mass forces and ignored lift-like forces – the main concern of Kelly & Hukkeri (2006). On the other hand, while Kelly's efforts (Kelly & Xiong 2010; Kelly, Pujari & Xiong 2012; Tallapragada & Kelly 2013, 2017) explicitly accounted for vortex shedding from the sharp trailing edge, his neat formulation treats the coupled vortex–body dynamics simultaneously; there is no means (no need) in his formulation to calculate hydrodynamic loads and their build up dynamics. Also, in the recent effort of Tallapragada & Kelly (2017), the authors showed that the Kutta condition is a non-holonomic constraint. Such a constraint is mainly on the body dynamics; i.e. the effect of the surrounding flow on the body is manifested by a non-holonomic constraint. In fact, the authors had a series of papers showing similarity between the dynamics of a swimming hydrofoil and the well-known non-holonomic system of the Chaplygin sleigh (Fairchild *et al.* 2011; Pollard, Fedonyuk & Tallapragada 2019).

In contrast to these efforts studying the locomotion of a hydrofoil (Kelly & Murray 2000; Morgansen *et al.* 2001; Morgansen, Vela & Burdick 2002; Vela *et al.* 2002; Kanso *et al.* 2005; Kelly & Hukkeri 2006; Tallapragada & Kelly 2017), we focus on the intrinsic unsteady aerodynamics of a pitching plunging wing. We develop a ROM of the buildup dynamics of unsteady lift and thrust that is (i) rich enough to capture the nonlinear effects at high angles of attack and high frequencies – to allow for non-trivial discoveries; and (ii) simple and compact enough to be amenable to geometric-control

analysis tools. We then bring the full power of geometric control and averaging to analyse such a dynamical system, aiming to discover unconventional nonlinear lift and thrust generation mechanisms. So, in contrast to the elegant geometric-mechanics efforts of Arnold and Marsden among others (Arnold 1966*b*, 1969; Marsden & Weinstein 1983; Holm *et al.* 1998; Bloch *et al.* 2000; Shashikanth *et al.* 2002; Shashikanth 2005; Borisov *et al.* 2003, 2007; Shashikanth *et al.* 2008; Kambe 2009), the current geometric-control analysis is more practically useful. The main objective is to present to the fluid dynamics audience how differential-geometric control is a heuristic analysis tool that points to unconventional and nonlinear mechanisms where one can scrutinize the flow dynamics using high-fidelity simulation (or experiment) to gain new physical insights.

In the next section, we present some background on how differential-geometric-control theory can help discover unconventional force generation mechanisms. We then pose the fluid mechanics problem statement to be tackled in this paper. In § 4, we discuss the characteristics of a ROM necessary for geometric-control analysis followed by our development of a geometric-control oriented ROM of the unsteady lift and thrust on a pitching–plunging wing. In § 5, we apply the proposed geometric control and averaging analysis to the developed ROM. In § 6, we perform numerical simulations of the URANS equations to validate the theoretical findings from geometric-control analysis; and to study the flow physics underlying the unconventional lift and thrust mechanisms suggested by geometric control. Finally, we provide a discussion in § 7.

2. Background: Lie brackets, periodic excitation and unconventional force generation

In this section, we present some aspects where geometric-control theory can be beneficial in the analysis of dynamical systems. Consider the nonlinear, control-affine system

$$\dot{x}(t) = f(x(t)) + \sum_{j=1}^{m} g_j(x(t))u_j(t), \quad x \in \mathbb{M}^n, \tag{2.1}$$

where x is the state vector evolving on an n-dimensional manifold $\mathbb{M}^n$, f is the drift vector field (uncontrolled dynamics), g_j represent the control vector fields corresponding to the inputs u_j. The main idea is that there can be no direct actuation leading to motion in a prescribed direction, although specific manipulation of the available actuators/controls may generate forces in that missed direction. This concept is generally referred to as anholonomy (Baillieul & Lehman 1996) or geometric phases (Marsden *et al.* 1991; Marsden 1997). For example, for driftless systems ($f = 0$), one can generate motion along the vector g_k by turning on the control input u_k and turning off all other controls. Geometric-control theory provides additional and non-intuitive directions to move along. These directions are determined through Lie bracket operations between the different control vectors. The Lie bracket between the two vectors g_j and g_k is defined as

$$[g_j, g_k] = \frac{\partial g_k}{\partial x} g_j - \frac{\partial g_j}{\partial x} g_k. \tag{2.2}$$

If the Lie bracket $[g_j, g_k]$ of two input vector fields is linearly independent of the two generating vectors g_j, g_k, then the implication is that, through some manipulation of the corresponding control inputs u_j, u_k, one can generate motion along a new direction: an unactuated direction over which there is no direct control authority. This is particularly useful to recover nonlinear controllability if linear controllability is lost. The motion along
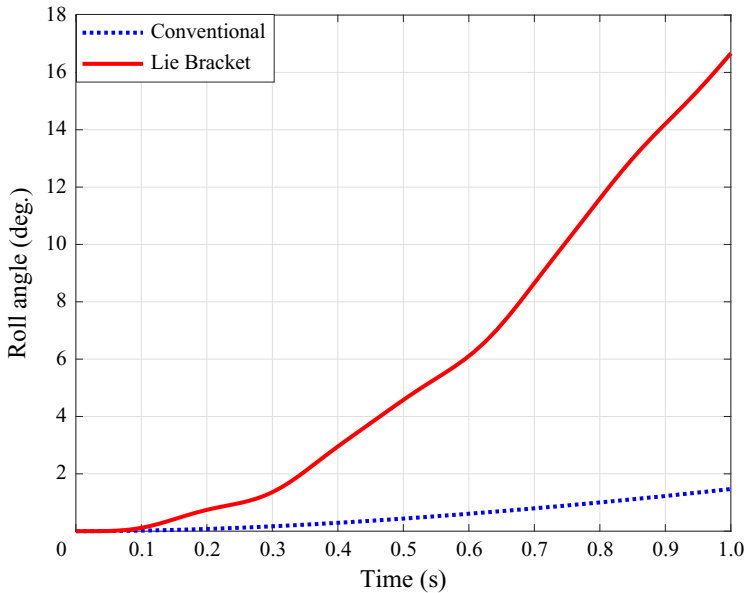
Figure 1. Numerical simulation of the NASA General Transport Model nonlinear flight dynamic model due to a 90°-phased aileron-elevator oscillations vs full aileron deflection near stall – to examine the roll response to the nonlinear Lie bracket roll mechanism vs the conventional one.

some Lie bracket vector $[\boldsymbol{g}_j, \boldsymbol{g}_k]$ can be realized by 90°-phased periodic signals for the corresponding inputs u_j and u_k (Murray & Sastry 1993; Liu 1997*a,b*).

A good example of an unconventional force-generation mechanism due to Lie bracketing (i.e. nonlinear interactions between control inputs) can be shown by recalling our recent efforts (Hassan & Taha 2017, 2021). In these efforts, the standard airplane flight dynamics was written in the form of (2.1). However, we retained all possible nonlinearities (aerodynamic and inertial) because the proposed differential-geometric-control analysis thrives on nonlinearities. One of the main features of geometric-control analysis is that it allows exploitation of nonlinearities rather than obviating them. It was shown that the Lie bracket between the elevator and aileron control inputs (i.e. pitch and roll control inputs for an airplane) possesses a much stronger rolling capability near stall in comparison with the conventional rolling mechanism using ailerons only. Figure 1 shows simulations over one second of the roll response of the NASA General Transport Model (Kwatny *et al.* 2012) near stall due to the nonlinear Lie bracket roll mechanism (i.e. 90°-phased sinusoids) in comparison with conventional roll with the maximum aileron deflection (Hassan & Taha 2021; Taha & Hassan 2021): an order-of-magnitude enhancement in the roll capability is achieved near stall via this nonlinear mechanism.

When combined with averaging theory, geometric control provides very useful tools for the analysis of periodically forced systems (Sarychev 2001; Bullo 2002; Vela 2003). It allows one to capture the higher-order effects due to interactions between periodic forcing and the system dynamics that are typically ignored by direct averaging (Maggia, Eisa & Taha 2019). These interactions may lead to force-generation mechanisms via symmetry breaking at high frequencies (Walsh & Sastry 1995; Marsden 1997). They may also lead to stabilizing actions: vibrational stabilization. A classical example is the Kapitza pendulum: an inverted pendulum whose pivot is subjected to vertical oscillations. The well-known unstable equilibrium of the inverted pendulum gains local asymptotic stability because
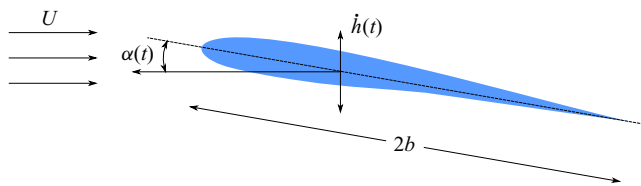
Figure 2. A schematic diagram for a pitching–plunging airfoil.

of the high-amplitude, high-frequency oscillations of the pivot. The reader is invited to watch the interesting video in ADCL (2019*a*) that clearly shows the vibrationally induced spring action on the Kapitza pendulum. Applying geometric-control-averaging analysis to the unstable flight dynamics of the hovering hawkmoth, we showed that its natural high-frequency periodic forcing induces a stabilizing pitch stiffness mechanism that could not be observed by direct averaging (Taha *et al.* 2015*a*, 2020). Indeed, it is an absolutely stunning design by Nature to make the very instinctive flapping motion of the wings, which is inevitably needed to produce the lift force that keeps the insect aloft, naturally stabilize the flight dynamics in a non-intuitive way without feedback (ADCL 2019*b*).

In fact, there have been several vibrational-stabilization-like concepts in the fluid mechanics literature, yet without making use of the geometric-control theory and averaging techniques mentioned above. The efforts of Jovanovic and his colleagues on turbulence suppression (Lieu, Moarref & Jovanović 2010; Moarref & Jovanović 2010) and turbulent drag reduction (Moarref & Jovanović 2012) in a channel flow through open-loop transverse wall oscillations are quite interesting examples that are relevant to the vibrational control tools mentioned above. Also, the vortex lock-in phenomenon (Karniadakis & Triantafyllou 1989; Young & Lai 2007) can be viewed as a form of vibrational stabilization for the Von Kármán vortex street instability.

3. Fluid mechanics problem statement

In this section, we present the fluid mechanics problem statement; the presentation is made such that the problem would be readily amenable to geometric-control analysis tools. Consider the problem of a harmonically pitching–plunging wing in the presence of a free stream U, as shown in figure 2. The pitching angle α (positive pitching up) and the plunging displacement h (positive downward) are written as

$$\alpha(t) = \alpha^* + A_\alpha \cos \omega t \quad \text{and} \quad h(t) = Hb \cos (\omega t + \phi), \quad (3.1a,b)$$

where ω is the oscillation frequency, α^* is the mean pitching angle, A_α is the amplitude of the pitching angle, H is the amplitude of the plunging displacement h normalized by the half-chord length b and ϕ is the phase difference between the two harmonic motions.

There are three objectives in this paper. First, we aim to develop a physics-based model that can predict the resulting unsteady lift $L(t)$, drag $\mathcal{D}(t)$ and separation point $x_s(t)$, where the corresponding coefficients are defined as

$$C_L = \frac{L}{\rho U^2 b} \quad \text{and} \quad C_D = \frac{\mathcal{D}}{\rho U^2 b}, \quad (3.2a,b)$$

where ρ is the fluid density. In this formulation, x_s represents the unsteady separation point as measured from the leading edge and normalized by the chord length; i.e. $0 \leqslant x_s \leqslant 1$.

The sought model must be (i) rich enough to capture the important physical aspects (e.g. nonlinear effects at high angles of attack and high frequencies), to allow

for non-trivial discoveries; and (ii) simple and compact enough to be amenable to geometric-control analysis tools; i.e. in the form of (2.1). Therefore, we propose the following form for the pitching–plunging wing:

$$\left.\begin{aligned} \dot{x}(t) &= f(x(t)) + g_h(x(t))\ddot{h}(t) + g_\alpha(x(t))\ddot{\alpha}(t) \\ y(t) &= [L(t) \quad \mathcal{D}(t) \quad x_s(t)]^{\mathrm{T}} = \Psi(x(t)), \end{aligned}\right\} \tag{3.3}$$

where x is a vector of internal aerodynamic states and y is the vector of output variables (e.g. lift and drag, and separation point). The vectors g_h, g_α are the input vector fields associated with plunging and pitching inputs, respectively. The function Ψ is a nonlinear function representing the output variables y in terms of the states x.

Accelerations $(\ddot{h}, \ddot{\alpha})$ are selected to be the inputs to facilitate the development of a proper dynamical-system representation where only direct dependence on inputs is allowed and not on their derivatives. Note that the aerodynamic loads depend on velocities and accelerations. Therefore, if velocities or positions were considered as inputs, the dynamical equations would depend on the derivatives of the inputs, deviating from the standard form (2.1). It should also be noted that the flow dynamics is indeed linear with respect to accelerations: Navier–Stokes equations (as well as Newton's equations) are linear in accelerations. Finally, it is noteworthy to mention that the above formulation can be easily extended to account for more inputs; e.g. surging $U(t)$. In this case, the input term $g_U(x)\dot{U}(t)$ would be added to (3.3) with the surging acceleration $\dot{U}(t)$ being the third control input.

Second, it is required to determine theoretical estimates of the averaged unsteady lift, drag and location of the separation point due to high-frequency, small-amplitude oscillations at arbitrary (high) angles of attack. We also assume a high speed U. Therefore, we have the following scaling argument:

$$A_\alpha = O(\epsilon), \quad H = O(\epsilon), \quad \omega = O(1/\epsilon), \quad U = O(1/\epsilon) \;\Rightarrow\; k = \frac{\omega b}{U} = O(1), \tag{3.4a–d}$$

where k is the reduced frequency and ϵ is a small bookkeeping parameter; e.g. terms multiplying ϵ^2 can be neglected with respect to those scaled by ϵ. Then, a geometric-control-averaging analysis will be applied to determine theoretical estimates of the cycle-averaged lift $\bar{C}_L$, drag $\bar{C}_D$, and separation point $\bar{x}_s$ to the leading order in ϵ. They will then be compared with the steady values corresponding to the mean angle of attack. For example, the cycle-averaged unsteady lift coefficient $\bar{C}_L$ will be compared with the steady lift coefficient $C_{L,s}(\alpha^*)$ at the mean angle of attack α^*; the difference represents lift enhancement or deterioration due to symmetry breaking. Also, the cycle-averaged separation point $\bar{x}_s$ will be compared with the steady value $x_0(\alpha^*)$ at the mean angle of attack; where $x_0(\alpha)$ represents the variation of the steady separation point with the static angle of attack. In this paper, the same oscillation frequency is used for both inputs (pitching and plunging), which is inherent in almost all averaging theorems and adopted in most of the unsteady fluid dynamic studies; only few studies have considered different frequencies for pitching and plunging (Webb, Dong & Ol 2008; Xiao & Liao 2010; Fenercioglu & Cetiner 2014). Third, the flow field will then be scrutinized, with the help of computational simulations, to obtain insights into the flow physics underlying these lift/drag enhancement/deterioration mechanisms.

They can have different frequencies, but averaging will be performed on the slowest frequency; the faster frequency can be one of its harmonics.

4. Physics-based reduced-order modelling of unsteady nonlinear aerodynamics

The main challenge precluding the application of geometric-control theory to fluid dynamics is that the latter is typically an infinite-dimensional system whereas the former was mainly developed for finite dimensional ones. It should be noted that there is a version of geometric-control theory for infinite dimensional systems, but of course with scant analysis tools in comparison with the finite-dimensional version. A practical geometric-control analysis would not only necessitate a finite-dimensional system, but also a relatively low-order one. Therefore, it cannot be directly applied to discretized Navier–Stokes equations where thousands or millions of states are typically used to describe the system. True reduced-order modelling is indispensable for a proper geometric-control analysis.

Inspecting the standard model reduction techniques available in the literature, we find that none of them can provide a satisfactory solution to the problem at hand. Ideally, the sought ROM should be in the form (2.1). Therefore, the model reduction technique must:

   (i) Yield a dynamical system that captures unsteadiness in the flow field. In this regard, quasi-steady and algebraic models are excluded no matter how accurate they are. Therefore, a feed forward neural network will not be satisfactory, even if it accurately captures the input–output map.

  (ii) Yield a nonlinear representation. Note that geometric-control tools thrive on nonlinearities. Therefore, the eigensystem realization algorithm (ERA) (Juang & Pappa 1985) and dynamic mode decomposition (DMD) (Rowley *et al.* 2009; Schmid 2010) will not be satisfactory for this objective because they strictly yield linear representations.

 (iii) Yield an analytical representation; an efficient 'simulation' tool is not the objective. Therefore, the Volterra series representation (Silva 1993; Raveh 2001) is not satisfactory for this objective, even though it may capture the nonlinear dynamical (unsteady) behaviour of the system in an efficient way.

In addition to the above absolutely necessary requirements, it is preferred that the model reduction technique (i) preserves the dynamical features of the system and (ii) be a data-driven approach that does not necessitate a prior knowledge of the system dynamical equations. The former may exclude proper orthogonal decomposition (POD) (Sirovich 1987; Lumley 2007) and the latter would also exclude POD and its balanced version (BPOD) (Rowley 2005). Also, while the extended DMD (EDMD) (Williams, Kevrekidis & Rowley 2015) may seem to satisfy all of the above requirements, it is not clear how it can yield a state space realization from the input–output data. It typically provides a relation (possibly nonlinear) between the state variables (or outputs), ignoring the input effects. Table 1 summarizes the pros and cons of each of the common model reduction techniques with respect to the requirements listed above. The above discussion indicates that the available standard model reduction techniques may not yield a ROM that allows proper nonlinear analysis, which invokes novel techniques for model reduction of fluid dynamics.

Until the sought model reduction technique is developed, a physics-based (phenomenological) approach is adopted here, which is a cornerstone in the present analysis. The main challenge is to represent the system in a form amenable to geometric-control analysis, e.g. the form (2.1). This objective necessitates a model that is (i) dynamical (i.e. captures unsteadiness), (ii) nonlinear and (iii) compact (i.e. in a state space form). This task is already very challenging; it has been a chronic problem

	POD	BPOD	ERA	DMD	Volterra
Dynamical Features	x	✓	✓	Somewhat	✓
Nonlinearity	✓	x	x	EDMD	✓
Data-Driven	x	x	✓	✓	✓
Analytical Representation	✓	✓	✓	✓	x
Input-Output Relation	✓	✓	✓	x	✓

Table 1. Comparison between the common model reduction techniques with respect to the listed requirements for the sought ROM.

in unsteady aerodynamics for a long time. One has to stress that it is the combination of the above three requirements that makes the problem elusive. For example, a compact quasi-steady model that captures nonlinear steady effects at high angles of attack can be easily obtained, but it would not capture unsteadiness. On the other hand, the unsteady aerodynamics community have developed several infinite-dimensional (e.g. Theodorsen 1935; Wagner 1925) and finite-dimensional (e.g. Leishman & Nguyen 1990; Peters 2008) representations of the unsteady lift dynamics, but these models are essentially linear and do not capture the nonlinear dynamics at large angles of attack. Of course, the Navier–Stokes equations govern the full unsteady nonlinear flow dynamics but are not in a compact form that is amenable to dynamical-systems theory in general or geometric-control theory in particular.

4.1. *Lift dynamics*

First, we focus on the lift dynamics; from which, we will construct the dynamics of drag/thrust and the separation point. Second, we follow a feedback linearization approach (Sastry 1999). In this approach, given a nonlinear dynamical system (2.1), the following question is addressed: does there exist (nonlinear) transformations $z = T(x)$ and $v = \beta(x, u)$ such that the dynamics in the transformed domain is linear: $\dot{z} = Az + Bv$ (Nijmeijer & Van der Schaft 1990)? That is, while the lift (and its dynamics) are essentially nonlinear with respect to the angle of attack (in the stall regime), does there exist a nonlinear map $v = \beta(x, \alpha)$ such that the lift dynamics is linear in v? Interestingly, although the seminal results of Von Kármán & Sears (1938) were developed approximately 40 years before the concept of feedback linearization (Brockett 1978; Jakubczyk & Respondek 1980), they can shed some light onto this question. Recall that, in the earlier efforts of Wagner (1925) and Theodorsen (1935), the authors wrote the main governing equation (integral equation of wake circulation) in terms of the normal speed of the airfoil

$$\frac{1}{2\pi b} \int_b^\infty \gamma_w(z, t) \sqrt{\frac{z+b}{z-b}} \mathrm{d}z = U \sin \alpha(t), \tag{4.1}$$

where b is the half-chord length, U is the forward speed of the airfoil and γ_w is the strength of the wake vortex sheet per unit span. Equation (4.1) is an infinite-dimensional linear dynamical system – represented by an integral equation in the wake circulation γ_w – whose input is the airfoil normal speed $U \sin \alpha(t)$. This formulation represents an impasse against generalization to unconventional lift mechanisms; it will always result in the classical lift coefficient $2\pi \sin \alpha$ with some transient (dynamics). In contrast, Von Kármán & Sears

(1938) arrived at a fundamentally different representation of the same dynamical system

$$\int_b^\infty \gamma_w(z,t)\sqrt{\frac{z+b}{z-b}}\mathrm{d}z = \Gamma_0(t), \tag{4.2}$$

where Γ_0 is the quasi-steady circulation

$$\Gamma_0(t) = UbC_{L,s}(\alpha(t)) + b^2 k_{\dot\alpha}\dot\alpha(t), \tag{4.3}$$

and $k_{\dot\alpha}$ is a coefficient for the rotational circulation, which depends on the hinge location (Dickinson, Lehmann & Sane 1999). It is well known that the lift dynamics resulting from the two dynamical systems (4.1)–(4.2) are identical. However, the first formulation is nonlinear in its input α while the latter is linear in its input Γ_0. That is, the nonlinear transformation (4.3) provides the sought feedback linearization; and Γ_0 represents the new input v. More importantly, the first formulation captures only the conventional lift mechanism (e.g. $2\pi \sin\alpha$) while the latter allows for unconventional (possibly nonlinear) lift mechanisms. To illustrate this point, recall that in (4.3) for the quasi-steady circulation, $C_{L,s}$ is the steady lift coefficient, which is a function of the angle of attack. This functional dependence $C_{L,s}(\alpha)$ is arbitrary, allowing treatment of unconventional lift mechanisms (e.g. a leading-edge vortex).

The main assumption in the present modelling effort is that the lift dynamics is linear in the quasi-steady circulation. That is, the circulatory lift can be written as

$$\left.\begin{aligned}\dot{\boldsymbol{x}}_c(t) &= [\boldsymbol{A}]_{n\times n}\boldsymbol{x}_c(t) + [\boldsymbol{B}]_{n\times 1}\Gamma_0(t) \\ L_C(t) &= \rho U\left\{[\boldsymbol{C}]_{1\times n}\boldsymbol{x}_c(t) + [D]_{1\times 1}\Gamma_0(t)\right\},\end{aligned}\right\} \tag{4.4}$$

where $\boldsymbol{x}_c \in \mathbb{R}^n$ represents the internal aerodynamic states used to realize such a linear dynamical system. The above assumption may not be a severe one given that no limitation is set on the nonlinear function $C_{L,s}(\alpha)$, the order n of the system (4.4) or its nature (i.e. stable/unstable); its eigenvalues may even change with the operating condition (i.e. with the mean angle of attack). In potential flow, such a system can be given by any suitable finite-dimensional approximation of Wagner or Theodorsen response functions – and $D = 1/2$ is the high-frequency gain (Taha & Rezaei 2020).

Since the focus here is to reconstruct the dynamics of the output, the nature (physical meaning) of the states $\boldsymbol{x}_c$ is not important. Note that one can always use a canonical similarity transformation $\boldsymbol{x}_{c,1} = \boldsymbol{T}\boldsymbol{x}_{c,2}$, where $\boldsymbol{T}$ is invertible, to transform between a given set of states $\boldsymbol{x}_{c,1}$ to another $\boldsymbol{x}_{c,2}$; in fact, we have infinitely many of these sets. While the internal aerodynamic states may not have an obvious physical meaning in many finite-dimensional approximations of the unsteady lift dynamics, few efforts presented realizations of the dynamical system (4.4) with states of physical relevance; Peters (2008) presented his model in terms of the Fourier coefficients/modes of the wake-induced normal velocity on the airfoil (inflow). In fact, the internal states of any realization of (4.4) can always be thought of as weighted modes of the wake vorticity.

Given (i) the steady $C_{L,s}$-α curve corresponding to some unconventional lift mechanism, and (ii) the airfoil motion represented by U and $\alpha(t)$, this approach provides the unsteady lift dynamics that captures such an unconventional lift mechanism. Figure 3 shows a schematic for this procedure. In fact, this approach was successfully adopted to model the unsteady nonlinear lift dynamics in insect flight (Taha *et al.* 2014). The model captures the leading-edge vortex (LEV) nonlinear contribution to lift in an unsteady fashion, relying on Wang's empirical formula for the steady lift due to a stabilized LEV: $C_{L,s} = A\sin 2\alpha$ (Wang, Birch & Dickinson 2004), where A is a constant. The unsteady model achieves
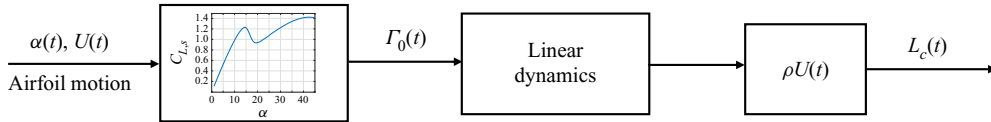
Figure 3. A schematic diagram for the circulatory lift dynamics and its linear dependence on the quasi-steady circulation.

such a challenging task with a very cheap computational cost and compact form (state space form).

The non-circulatory lift L_{NC} can be easily modelled linearly in the normal acceleration $a_{1/2}$ of the mid-chord point

$$L_{NC}(t) = m_v a_{1/2}(t) \cos \alpha(t), \tag{4.5}$$

where m_v is the virtual (added) mass, which is given by $m_v = \pi \rho b^2$ in a potential-flow setting, and the airfoil normal acceleration is given by

$$a_{1/2}(t) = \frac{\mathrm{d}}{\mathrm{d}t} \left(U \sin \alpha(t) + \dot{h}(t) \cos \alpha(t) - ab\dot{\alpha}(t) \right), \tag{4.6}$$

where the hinge location is at a distance ab behind the mid-chord point. The relation (4.5) would make the output (lift) have a direct dependence on the input (acceleration); i.e. $\boldsymbol{\Psi}$ would have dependence on the input $\boldsymbol{u}$ as well as the states $\boldsymbol{x}$. Furthermore, from a different perspective, our recent efforts indicate that viscosity induces a phase lag between the normal acceleration and the non-circulatory lift force (Taha & Rezaei 2020). Therefore, we introduce a first-order lag between the two

$$\left.\begin{aligned} \tau_v \dot{x}_v(t) + x_v(t) &= a_{1/2}(t) \\ L_{NC}(t) &= m_v x_v(t) \cos \alpha(t), \end{aligned}\right\} \tag{4.7}$$

where τ_v is the time constant of such a dynamics. That is, the normal acceleration $a_{1/2}$ does not impact the non-circulatory lift L_{NC} instantaneously (i.e. through an algebraic relation: (4.5)). Instead, it affects L_{NC} after passing through a first-order lag whose internal state is x_v.

One must stress that the above modelling approach is not meant to provide an accurate quantitative assessment of the unsteady nonlinear lift dynamics in the stall regime. Rather, this modelling approach is conceptual/qualitative. For example, conceptually, the non-circulatory lift is indeed proportional to the airfoil acceleration, and the proportionality constant (m_v) is not stipulated here; it can take any arbitrary value. In fact, its value is irrelevant for the intended symbolic analysis; it would rather serve as a bookkeeping parameter. That is, a resulting term proportional to m_v would imply that it is due to added/virtual mass effects; another term proportional to $k_{\dot{\alpha}}$ would point to rotational contributions. Similarly, the steady $C_{L,s}$-α curve can assume any shape; a term proportional to $\mathrm{d}C_{L,s}/\mathrm{d}\alpha$ would point to the role of the lift curve slope, and so on. Moreover, the dynamics between Γ_0 and L_C can take an arbitrary order n or nature (arbitrary $\boldsymbol{A}, \boldsymbol{B}, \boldsymbol{C}, \boldsymbol{D}$). From this conceptual perspective, the above model is credible for the ensuing symbolic analysis; the specific values of the model parameters ($n, \boldsymbol{A}, \boldsymbol{B}, \boldsymbol{C}, \boldsymbol{D}, C_{L,s}(\alpha), k_{\dot{\alpha}}, m_v, \tau_v$) are irrelevant.

Recall that one can always use a canonical similarity transformation to transform a given linear system into a special form, we assume without loss of generality (to simplify

symbolic computations) that the linear model (A, B, C, D) is in the observable canonical form (Ogata & Yang 1970)

$$
A = \begin{bmatrix} 0 & \cdots & 0 & -a_0 \\ 1 & \cdot & 0 & -a_1 \\ \vdots & \ddots & \vdots & \vdots \\ 0 & \cdots & 1 & -a_{n-1} \end{bmatrix}, \quad B = \begin{pmatrix} b_0 - b_n a_0 \\ b_1 - b_n a_1 \\ \vdots \\ b_{n-1} - b_n a_{n-1} \end{pmatrix}, \left.\begin{array}{c} \\ \\ \\ \\ \end{array}\right\}
$$
$$
C = [0 \quad \ldots \quad 0 \quad 1], \quad D = b_n, \qquad (4.8)
$$

where the coefficients a and b are the coefficients of the denominator and numerator of the corresponding transfer function

$$
\frac{L_C}{\rho U \Gamma_0}(s) = \frac{b_n s^n + b_{n-1} s^{n-1} + \cdots + b_1 s + b_0}{s^n + a_{n-1} s^{n-1} + \cdots + a_1 s + a_0}. \qquad (4.9)
$$

From a dynamical-system perspective, the ratio b_0/a_0 is the steady-state (DC) gain of the system: the ratio of the steady-state output (lift) to the input $\rho U \Gamma_0$. Clearly, this is unity by construction. Therefore, in the ensuing symbolic computations, b_0 is taken equal to a_0. Also, $D = b_n$ is the high-frequency gain k_{hf} of the system.

4.2. *Drag/thrust dynamics*

Continuing with the conceptual modelling approach, and ignoring the skin friction drag, the pressure drag is typically given by

$$
\mathcal{D}(t) = L(t) \tan \alpha(t) - F_S(t), \qquad (4.10)
$$

where L is the total lift force ($L = L_C + L_{NC}$) and F_S is the leading-edge suction force. Indeed, without leading-edge suction, the resultant force N is normal to the wing (Schlichting & Truckenbrodt 1979); the lift and drag would be given as $N \cos \alpha$ and $N \sin \alpha$, respectively; i.e. $\mathcal{D} = L \tan \alpha$.

The dynamics of the first drag term ($L \tan \alpha$) is automatically linked to the lift dynamics. Interestingly, the dynamics of the second term (the suction force F_S) can also be connected with the circulatory lift dynamics. Using potential-flow aerodynamics, Garrick (1937) wrote the suction force as

$$
F_S(t) = 2\pi \rho b \left[v_{3/4}(t) C(k) - \frac{b}{2} \dot{\alpha}(t) \right]^2, \qquad (4.11)
$$

where $v_{3/4}$ is the airfoil normal speed at the three-quarter chord and $C(k)$ is Theodorsen's lift frequency response function (Theodorsen 1935), which is given in terms of the reduced frequency k as

$$
C(k) = \frac{H_1^{(2)}(k)}{H_1^{(2)}(k) + i H_0^{(2)}(k)}, \qquad (4.12)
$$

where $H_n^{(m)}$ is the Hankel function of the mth kind of order n. Note that the multiplication $v_{3/4}(t) C(k)$ in (4.11) is traditionally interpreted as the output of the transfer function whose frequency response is $C(k)$ due to the input signal $v_{3/4}$; i.e. it is the unsteady version of $v_{3/4}$.

To generalize Garrick's relation (4.11), we replace $v_{3/4}$ with the quasi-steady circulation $\Gamma_0/(2\pi b)$, as done with the lift dynamics above. Moreover, its unsteady version $v_{3/4} C(k)$

928 A30-14

will be replaced by the unsteady version of Γ_0; i.e. the output of the dynamical system (4.4): $\boldsymbol{Cx}_c + D\Gamma_0$. As such, the suction force is modelled in this conceptual approach as

$$F_S(t) = k_S \rho b \left[\frac{\boldsymbol{Cx}_c(t) + D\Gamma_0(t)}{2\pi b} - \frac{b}{2}\dot{\alpha}(t) \right]^2, \tag{4.13}$$

where k_S is a coefficient of suction: bookkeeping parameter for suction; its potential-flow value is $k_S = 2\pi$.

4.3. *Dynamics of the separation point*

Unsteady separation is a complex phenomenon whose dynamics is quite difficult to model. In fact, a mere criterion for unsteady separation is controversial – the common criterion of vanishing shear is not accurate (Sears 1956). However, as stated above, the intent is not to develop a quantitative model for accurate prediction, but rather a conceptual model. A fairly straightforward conceptual model of the dynamics of the separation point is that of Goman & Khrabrov (1994). Simply, the unsteady separation point x_s follows the steady one x_0 (which is a function of the angle of attack) via a simple lag τ_1 and a delay τ_2

$$\tau_1 \dot{x}_s(t) + x_s(t) = x_0 \left(\alpha(t) - \tau_2 \dot{\alpha}(t) \right). \tag{4.14}$$

In this conceptual model, the specific values of τ_1, τ_2 are irrelevant; the functional dependence $x_0(\alpha)$ is arbitrary. Moreover, to relate the dynamics of separation to the lift dynamics, we adopt the Kirchhoff steady model, which relates a nonlinear lift coefficient to separation

$$C_{L,s}(\alpha) = 2\pi \sin \alpha \left(\frac{1 + \sqrt{x_0(\alpha)}}{2} \right)^2. \tag{4.15}$$

That is, given a steady C_L-α curve, $C_{L,s}(\alpha)$, the corresponding variation, $x_0(\alpha)$, of the separation point with the angle of attack can be determined from the Kirchhoff model (4.15).

4.4. *The final dynamical ROM*

Applying the above conceptual modelling efforts to a pitching–plunging wing, any dependence on the angle of attack α would be replaced by the effective angle of attack: $\alpha_{eff} = \alpha + \arctan(\dot{h}/U)$, where h is positive downward. As such, the quasi-steady circulation is written as

$$\Gamma_0(\alpha, \dot{\alpha}, \dot{h}) = UbC_{L,s} \left(\alpha(t) + \arctan \frac{\dot{h}(t)}{U} \right) + b^2 k_{\dot{\alpha}} \dot{\alpha}(t). \tag{4.16}$$

Let us summarize the assumptions behind the developed model:

(i) The dynamics (due to vortex shedding) from the quasi-steady circulation Γ_0 (the input) to the circulatory lift L_C (the output) is linear (4.4), but arbitrary.

(ii) The quasi-steady circulation Γ_0 is given by (4.16) for a pitching–plunging wing, where $C_{L,s}(\alpha)$ is the steady lift curve, which depends arbitrarily (nonlinearly) on the angle of attack α.

(iii) The non-circulatory lift L_{NC} depends linearly on the wing's normal acceleration at the half-chord point with a simple lag (4.7).

(iv) The dynamics of the skin friction drag is neglected; hence, the unsteady drag $\mathcal{D}$ is constructed from the unsteady lift L and suction force F_S (4.10).

(v) The unsteady suction force can be determined from the circulatory lift dynamics (4.13).

(vi) The Goman–Khrabrov model (4.14) of unsteady separation is adopted; and the steady location $x_0(\alpha)$ of the separation point is determined from the arbitrary steady lift curve $C_{L,s}(\alpha)$ according to the Kirchhoff model (4.15).

Combining all these elements, we write the following ROM of the unsteady nonlinear aerodynamics of a pitching–plunging wing:

$$
\frac{\mathrm{d}}{\mathrm{d}t}
\begin{pmatrix} x_c \\ x_v \\ x_s \\ \alpha \\ \dot{\alpha} \\ \dot{h} \end{pmatrix}
=
\begin{pmatrix}
A x_c + B \Gamma_0(\alpha, \dot{\alpha}, \dot{h}) \\
\dfrac{-1}{\tau_v}\left[x_v + \left(U\cos\alpha - \dot{h}\sin\alpha \right)\dot{\alpha} \right] \\
\dfrac{-1}{\tau_1}\left[x_s - x_0\left(\alpha + \arctan\dfrac{\dot{h}}{U} - \tau_2\dot{\alpha} \right) \right] \\
\dot{\alpha} \\
0 \\
0
\end{pmatrix}
+
\begin{pmatrix}
\mathbf{0}_{n\times 1} \\
\dfrac{ab}{\tau_v} \\
0 \\
0 \\
1 \\
0
\end{pmatrix}
u_\alpha
$$

$$
+
\begin{pmatrix}
\mathbf{0}_{n\times 1} \\
\dfrac{\cos\alpha}{\tau_v} \\
0 \\
0 \\
0 \\
1
\end{pmatrix}
u_h,
\tag{4.17}
$$

which can be written in an abstract form as

$$
\dot{x}(t) = f(x(t)) + g_\alpha(x(t))u_\alpha(t) + g_h(x(t))u_h(t),
\tag{4.18}
$$

where $x = [x_c, x_v, x_s, \alpha, \dot{\alpha}, \dot{h}]$ is the state vector of dimension $n + 5$, and the control inputs u_α, u_h are the pitching and plunging accelerations $\ddot{\alpha}$, $\ddot{h}$, respectively. The system (4.17) is exactly in the form (2.1), which is amenable to geometric-control analysis. The output equation is written as

$$
\left.
\begin{aligned}
L(t) &= \Psi_L(x(t)) = \rho U \left(C x_c(t) + D\Gamma_0(\alpha, \dot{\alpha}, \dot{h}) \right) + m_v x_v(t)\cos\alpha(t), \\
\mathcal{D}(t) &= \Psi_D(x(t)) = L(t)\tan\alpha(t) - k_S \rho b \left(\frac{C x_c(t) + D\Gamma_0(\alpha, \dot{\alpha}, \dot{h})}{2\pi b} - \frac{b}{2}\dot{\alpha}(t) \right)^2, \\
x_s(t) &= \Psi_s(x(t)) = x_s(t).
\end{aligned}
\right\}
\tag{4.19}
$$

5. Combined geometric-control-averaging analysis of the unsteady fluid dynamics problem

There are several types of geometric-control analysis that can be applied to the ROM (4.18). These include (i) a nonlinear controllability analysis by computing the accessibility distribution at some point x_0 corresponding to some mean angle of attack; (ii) a Fliess functional expansion (Fliess, Lamnabhi & Lamnabhi-Lagarrigue 1983; Isidori 1995), which provides the early response of the control-affine system (2.1), equivalently (4.18) – the reader is referred to the work of Pla Olea (2019) for such an analysis; and (iii) a combined geometric-control-averaging analysis (e.g. Maggia *et al.* 2019; Bullo 2002).

In this work, we opt to perform this last type since it provides a constructive technique to perform rigorous averaging of the system (4.18) when subjected to periodic forcing – relating properties of the averaged dynamics to the original time-periodic system. Hence, it will allow identification of enhancement in the mean lift and thrust beyond the steady values.

Let us introduce time-periodic pitching–plunging

$$u_\alpha = \ddot{\alpha} = \omega^2 A_\alpha \cos \omega t, \quad u_h = \ddot{h} = \omega^2 H b \cos(\omega t + \phi), \qquad (5.1a,b)$$

where ω is the oscillation frequency, A_α is the amplitude of the pitching angle (or angle of attack) α, H is the amplitude of the plunging displacement h normalized by the half-chord length b and ϕ is the phase difference between the two harmonic motions. Moreover, a scaling argument is necessary before applying the averaging theorem. Therefore, we focus our analysis on low-amplitude, high-frequency airfoil oscillations, flying at a high speed U

$$A_\alpha = O(\epsilon), \quad H = O(\epsilon), \quad \omega = O(1/\epsilon), \quad U = O(1/\epsilon) \Rightarrow k = \frac{\omega b}{U} = O(1),$$
$$(5.2a\text{–}d)$$

where k is the reduced frequency and ϵ is a small parameter; e.g. terms multiplying ϵ^2 can be neglected with respect to those scaled by ϵ. Substituting the inputs u_α, u_h from (5.1a,b) into the system (4.18), and applying this scaling argument, one obtains

$$\dot{x}(t) = f(x(t)) + \frac{1}{\epsilon} \left(A_\alpha g_\alpha(x(t)) \cos \omega t + H b g_h(x(t)) \cos(\omega t + \phi) \right). \qquad (5.3)$$

This system is a high-amplitude, high-frequency, nonlinear, time-varying system whose analysis is challenging. First of all, direct averaging of the system (5.3) is futile because it will completely neglect the effect of pitching–plunging oscillations on the averaged dynamics; the cosine signal has a zero mean. In fact, averaging must be discreetly and rigorously performed; the statement by Sanders, Verhulst & Murdock (2007) on the subtleties of averaging is quite expressive: 'To many physicists and astronomers averaging seems to be such a natural procedure that they do not even bother to justify the process. However, it is important to have a rigorous approximation theory, since it is precisely the fact that averaging seems so natural that obscures the pitfalls and restrictions of the method'.

In Appendix A, we list some rigorous mathematical tools for averaging from which we present below a specific theorem that is especially suited for the averaging analysis of the above system.

5.1. *A special technique for averaging of high-amplitude periodically forced nonlinear systems*

Consider a nonlinear system subjected to a high-frequency, high-amplitude, periodic forcing in the form

$$\dot{x}(t) = f(x(t)) + \frac{1}{\epsilon} G\left(x(t), \frac{t}{\epsilon}\right). \qquad (5.4)$$

THEOREM A.1. *If G is a T-periodic, zero-mean vector field and both f, G are continuously differentiable, then the averaged dynamical system corresponding to the system ([A3a,b](#)) is written as*

$$\dot{\bar{x}}(t) = \bar{F}(\bar{x}(t)), \tag{5.5}$$

where $\bar{F}(\bar{x}(t)) = (1/T) \int_0^T F(x(t), \tau) \, d\tau$, and F is the pullback of f along the flow Φ_t^G of the time-varying vector field G.

Using the chronological calculus formulation of Agrachev & Gamkrelidze ([1978](#)), Bullo ([2002](#)) showed that, for a time-invariant f and time-varying G, the pullback vector field $F(x(t), t)$ can be written explicitly in terms of iterated Lie brackets of f and G as

$$F(x(t), t) = f(x(t)) + \sum_{k=1}^{\infty} \int_0^t \cdots \int_0^{s_{k-1}} \left(ad_{G(x(t),\, s_k)} \ldots ad_{G(x(t),s_1)} f(x) \right) ds_k \ldots ds_1, \tag{5.6}$$

where $ad_G f = [G, f]$.

5.2. *Application to the unsteady fluid dynamics system*

In this section, we apply the above averaging theorem to the developed ROM ([4.17](#)), equivalently ([4.18](#)) or ([5.3](#)). In particular, we use the series ([A5](#)) to obtain the pullback vector field F as

$$F(x, t) = f(x) + \mathcal{G}(x, t), \tag{5.7}$$

where

$$\mathcal{G}(x, t) = \sum_{j=\alpha,h} [g_j, f] \int_0^t u_j(s_1) \, ds_1$$

$$+ \sum_{j=\alpha,h} \sum_{\ell=\alpha,h} [g_j, [g_\ell, f]] \int_0^t \int_0^{s_1} u_j(s_1) u_\ell(s_2) \, ds_2 \, ds_1 + \ldots \tag{5.8}$$

As such, the averaged dynamics is written as

$$\frac{d}{dt} \begin{pmatrix} \bar{x}_c \\ \bar{x}_v \\ \bar{x}_s \\ \bar{\alpha} \\ \dot{\bar{\alpha}} \\ \bar{h} \end{pmatrix} = \begin{pmatrix} A\bar{x}_c + B\Gamma_0(\bar{\alpha}, \dot{\bar{\alpha}}, \bar{h}) \\ \dfrac{-1}{\tau_v} \left[\bar{x}_v + \left(U\cos\bar{\alpha} - \bar{h}\sin\bar{\alpha} \right) \dot{\bar{\alpha}} \right] \\ \dfrac{-1}{\tau_1} \left[\bar{x}_s - x_0 \left(\bar{\alpha} + \arctan\dfrac{\bar{h}}{U} - \tau_2\dot{\bar{\alpha}} \right) \right] \\ \dot{\bar{\alpha}} \\ 0 \\ 0 \end{pmatrix} + \begin{pmatrix} \bar{\mathcal{G}}_{1\rightarrow n}(\bar{\alpha}) \\ 0 \\ \bar{\mathcal{G}}_{n+2}(\bar{\alpha}) \\ 0 \\ 0 \\ 0 \end{pmatrix}, \tag{5.9}$$

where $\bar{\mathcal{G}}_{1\rightarrow n}$ are the first n components of the cycle average of the vector field $\mathcal{G}$, and $\bar{\mathcal{G}}_{n+2}$ is the $(n+2)$th-entry. It is found that these components are the only non-zero entries of $\bar{\mathcal{G}}$ and that they depend only on the angle of attack.

Having obtained the averaged dynamics ([5.9](#)) of the unsteady fluid dynamical system ([4.17](#)), we need to study its equilibrium – the averaging theorem above relates properties of the original nonlinear time-periodic (NLTP) system to equilibrium of the

averaged dynamics. That is, we set the left-hand side of (5.9) to zero and solve for x^* that satisfies the equation; i.e. we have

$$f(x^*) + \bar{\mathcal{G}}(x^*) = 0. \tag{5.10}$$

Noting that the last three components of $\mathcal{G}$ are zeros, it implies that equilibria of the last two states $(\bar{\alpha}, \bar{h})$ are automatically satisfied; and equilibrium of the $\bar{\alpha}$-dynamics stipulates that $\dot{\alpha}^* = 0$, which is intuitively expected. This result, in addition to $\mathcal{G}_{n+1} = 0$ implies that equilibrium of $\bar{x}_v$ is attained at $x_v^* = 0$. It remains to solve for x_c^* and x_s^*. Taking $\dot{h}^* = 0$, leaving α^* arbitrary (to study the effect of the mean angle of attack) and realizing that the first n and the $n + 2$ components of $\mathcal{G}$ depend only on α, we obtain

$$\left.\begin{aligned} x_c^* &= -[A]^{-1}\left(\bar{\mathcal{G}}_{1\to n}(\alpha^*) + UbC_{L,s}(\alpha^*)B\right) \\ x_s^* &= x_0(\alpha^*) + \tau_1 \mathcal{G}_{n+2}(\alpha^*). \end{aligned}\right\} \tag{5.11}$$

Having solved for the equilibrium point x^* of the averaged dynamics (5.9), we perform averaging of the output variables (lift, drag and separation point), which are nonlinear functions of the states x. Due to these nonlinearities, the average of an output function $\Psi_m(x)$, $m \in \{L, D, s\}$, is not simply $\Psi_m(x^*)$. As a first-order approximation, each state x_i, $i \in \{1, \ldots, n + 2\}$, can be written as $x_i(t) = x_i^* + A_{x_i}\cos(\omega t + \phi_i)$. Hence, we expand each output function Ψ_m around x^* in a Taylor series expansion and average over the cycle to obtain

$$\bar{\Psi}_m = \Psi_m(x^*) + \sum_{i=1}^{n+5}\sum_{q=1}^{n+5} \frac{\partial^2 \Psi_m}{\partial x_i \partial x_q} \frac{A_{x_i}A_{x_q}}{2} \cos(\phi_i - \phi_q) + \ldots \tag{5.12}$$

5.3. *Averaged lift*

Applying the averaging analysis above to the lift output variable Ψ_L and normalizing by $\rho U^2 b$, we obtain

$$\bar{C}_L = C_{L,s}(\alpha^*) + \tfrac{1}{4}\left(H^2 k^2 + k_{hf}A_\alpha^2\right)C_{L,s}''(\alpha^*) + O(\epsilon^4; m_v, A_\alpha), \tag{5.13}$$

where the infinite series is truncated after $O(\epsilon^2)$. The result (5.13) is quite revealing. Recall that $\bar{C}_L$ represents the mean of the unsteady lift coefficient due to the pitching–plunging inputs (5.1*a,b*) and $C_{L,s}(\alpha^*)$ is the (mean) steady lift coefficient at the mean angle of attack α^*. From a linear system perspective, they may be equal – oscillating the airfoil around a mean angle of attack results in a periodic lift whose mean corresponds to the steady lift at the mean angle of attack. As such, the difference between the two would represent lift enhancement/deficiency. The present analysis implies that, to the leading order, the lift enhancement due to pitching and/or plunging is proportional to the curvature $C_{L,s}'' \equiv \mathrm{d}^2 C_{L,s}/\mathrm{d}\alpha^2$ of the steady lift curve. Aerodynamicists typically concern themselves with the slope $C_{L,s}'$ of such a curve; perhaps, this is the first time the role of its curvature has been pointed out. Moreover, the analysis revealed a higher-order pitching contribution to lift enhancement, which is due to added-mass effects: the last term $O(\epsilon^4; m_v, A_\alpha)$ is proportional to A_α and m_v.

The above result is quite interesting in the sense that it identifies the role of the curvature $C_{L,s}''$ of the steady lift curve in controlling lift enhancement due to high-frequency, low-amplitude pitching–plunging. Since $C_{L,s}''$ is almost zero in the small-α linear regime, this result points to potential lift enhancement/deficiency in the stall and post-stall regimes:
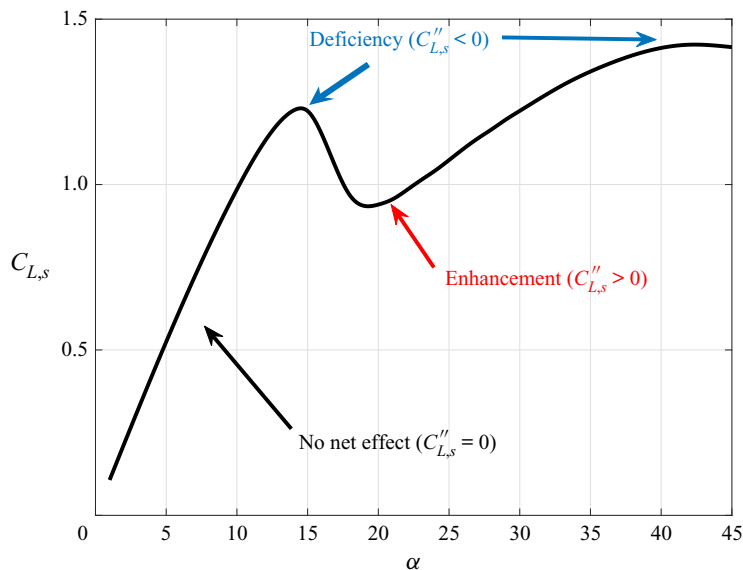
Figure 4. The curvature $C''_{L,s}$ of the steady lift curve controls lift enhancement due to high-frequency, low-amplitude pitching–plunging. Note that the angles of attack at the peaks and troughs of the $C_{L,s}$-α curve change with R. The curve reported here is for $R = 500\,\mathrm{K}$ for which the angles of attack at the peaks and troughs are $15°$ and $20°$, respectively. For a smaller R (in the range of $10\,000$–$60\,000$), they would be smaller (approximately $10°$ and $15°$, respectively).

lift deficiency near the peak(s) in the stall regime; and lift enhancement near the trough in the post-stall regime, as shown in figure 4. In fact, there have been numerous experimental and computational studies on the lift dynamics due to pitching and/or plunging in the stall regime (e.g. Carr 1988; Lee & Gerontakos 2004; Andro & Jacquin 2009; Rival & Tropea 2010; Cleaver *et al.* 2011, 2012, 2013; Baik *et al.* 2012; Choi *et al.* 2015; Chiereghin *et al.* 2019; Gupta & Ansell 2019). However, none of these efforts revealed this role of $C''_{L,s}$.

Focusing on the relevant studies corresponding to small-amplitude, high-frequency oscillations around the peaks and troughs of the steady lift curve, we find them corroborating the current result. In fact, as early as the efforts of McCroskey *et al.* (1982), one can observe this behaviour. For example, figure 6 of Carr (1988) shows a 4 % lift deficiency due to pitching around the peak. All other cases were either performed at large amplitudes or low frequencies. More recently, the efforts of Rival & Tropea (2010) studying plunging of the SD 7003 airfoil at $R = 60\,000$ around $\alpha^* = 0°, 5°, 8°, 10°$ also yielded similar results. Inspecting figure 4(*a*) in their effort, we find little-to-no change between the mean lift coefficient $\bar{C}_L$ and the steady lift coefficient $C_{L,s}(\alpha^*)$ at the mean angle of attack in the cases of plunging in the linear regime ($\alpha^* = 0, 5$); and a lift decrease in the cases of plunging near the peak in the stall regime: 26 % in the $\alpha^* = 8°$ case, and 13 % in the $\alpha^* = 10°$ case. Note that the peak of the steady $C_{L,s}$-α curve is at $10°$ in this case. In general, the angles of attack at the peaks and troughs of the $C_{L,s}$-α curve change with R; they increase when R is increased. Also, the results of Cleaver *et al.* (2011) are quite clear in this regard; they performed a plunging experiment of NACA 0012 at $R = 10\,000$ around $\alpha^* = 15°$, which corresponds to the trough of the $\bar{C}_L$-α curve at this value of R (Chiereghin *et al.* 2019). They observed significant lift enhancement in these conditions, which increases with the plunging amplitude, reaching up to 310 % (see figure 11 in their effort). The same group performed a more comprehensive study (Chiereghin *et al.* 2019)

investigating enhancement/deficiency in the mean and amplitude of the unsteady lift on a plunging NACA 0012 at $R = 20\,000$ with different amplitudes, frequencies and mean angles of attack. Investigating figure 7 in their effort and confining ourselves to small amplitudes, one finds: (i) almost no net change in the mean lift coefficient when plunging in the linear regime at $\alpha^* = 0$, $5°$; (ii) a small deficiency in the mean lift coefficient when plunging at $\alpha^* = 9°$, which is the peak of the $\bar{C}_L$-α curve; and (iii) a significant enhancement in the mean lift coefficient when plunging at $\alpha^* = 15°$, which is the trough of the $\bar{C}_L$-α curve. Indeed, these experimental results corroborate the current theoretical finding on the role of the curvature $C''_{L,s}$ of the steady lift curve in controlling lift enhancement, which will be validated in more detail below using relatively high-fidelity computational simulations (URANS).

Finally, it should be noted that the efforts of Cleaver *et al.* (2012, 2013), although concerned with lift enhancement/deficiency, do not apply here since their observed bifurcations in the mean lift coefficient were at quite high Strouhal numbers (frequencies). Note that increasing the frequency (even with keeping the plunging amplitude fixed) leads to an increase in the effective angle of attack. Therefore, even though the current analysis and results should be valid for high frequencies, there is a limitation on the frequency in the plunging case; for a given plunging amplitude, the maximum frequency should be set to maintain the effective angle of attack within the intended range of $C''_{L,s}$. For example, Cleaver *et al.* (2012) interestingly observed a bifurcation in the mean lift coefficient leading to a significant lift enhancement when plunging at $\alpha^* = 0$. However, this behaviour is not attained until a quite high Strouhal number of 2 (i.e. $k = 2\pi$) is reached at $H = 0.2$, which corresponds to an effective angle of attack in the range $\pm \arctan kH = \pm51.5°$. Clearly, this is outside the scope of our analysis.

5.4. *Averaged drag/thrust*

Applying the averaging analysis above to the drag output variable Ψ_D due to a plunging input, and normalizing by $\rho U^2 b$, we obtain

$$\bar{C}_D = C_{D,s}(\alpha^*) + \frac{H^2 k^2}{4} \underbrace{\left[C''_{L,s} \tan\alpha - \frac{k_S}{2\pi^2} \left(C_{L,s} C''_{L,s} + k_{hf}^2 C'^2_{L,s} \right) \right]_{\alpha=\alpha^*}}_{-\chi_T} + O(\epsilon^3), \quad (5.14)$$

where the infinite series is truncated after $O(\epsilon^2)$. The result (5.14) is also quite revealing in the sense that any difference between $\bar{C}_D$ and $C_{D,s}(\alpha^*)$ would represent either a drag increase or decrease (i.e. thrust production). The analytical nature of the current study presents itself here. For example, the last term $(-(k_S k_{hf}^2/2\pi^2)C'^2_{L,s})$ between the square brackets is negative indicating thrust production, proportional to the lift curve slope $C'_{L,s}$ (i.e. active in the linear regime), and proportional to the bookkeeping parameter k_S (i.e. due to suction). Therefore, it represents the classical thrust-production mechanism in the linear regime due to plunging. In fact, when using potential-flow characteristics: $k_S = 2\pi$, $C'_{L,s} = 2\pi$, and recalling that k_{hf} is the high-frequency gain of the lift transfer function (i.e. Theodorsen's $C(k)$), this term reduces to Garrick's potential-flow result on the mean thrust coefficient C_T due to plunging (Garrick 1937; Taha 2018)

$$C_T = \pi H^2 k^2 |C(k)|^2. \quad (5.15)$$

Therefore, the current result represents a high-frequency generalization of Garrick's classical result to regimes with an arbitrary lift dynamics (not necessarily governed by
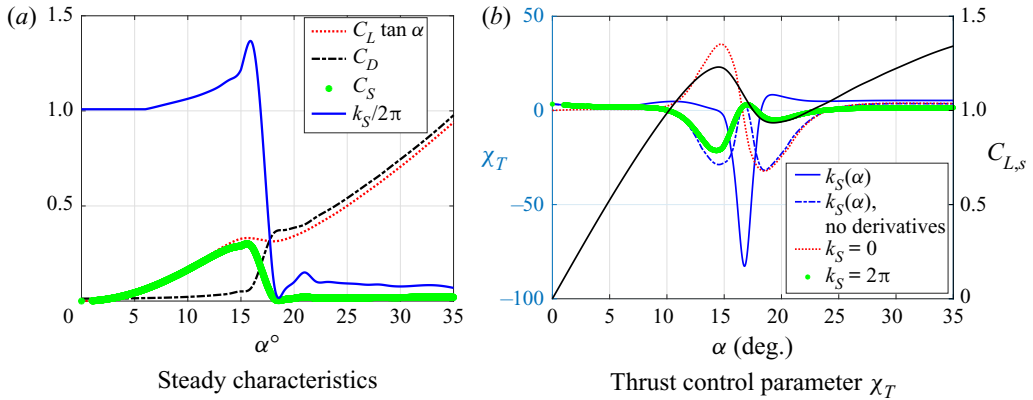
Figure 5. URANS simulations of NACA 0012 at $R = 500$ K at different static angles of attack along with the variation of the thrust control parameter χ_T due to low-amplitude, high-frequency plunging with the mean angle of attack.

Theodorsen) and unconventional lift mechanisms (not necessarily the classical $2\pi \sin \alpha$). Hence, more contributions are revealed in our result in (5.14) besides Garrick's. In particular, the first two terms are quite interesting as they point to a nonlinear thrust generation mechanism in the stall or post-stall regime where the effect of $C_{L,s}''$ is prominent. The former indicates an increased drag inherited from lift enhancement in regions of positive curvature and *vice versa* (i.e. an increase in the resultant normal aerodynamic force, similar to the findings of Choi *et al.* 2015). The latter is due to suction and is opposing to the former: it would provide thrust production in regions of positive curvature. Since these two contributions are competing, we performed the following study to assess the role of the curvature $C_{L,s}''$ of the lift curve in drag increase or thrust production.

We performed a URANS simulation (detailed below) of a NACA 0012 at $R = 500$ K at different static angles of attack to obtain the mean lift and drag coefficients $C_{L,s}$, $C_{D,s}$, as shown in figure 5(*a*). Indeed, in the absence of leading edge suction, the resultant force (ignoring skin friction) is normal to the wing surface (Schlichting & Truckenbrodt 1979), leading to the geometric relation $C_D = C_L \tan \alpha$ between the lift and drag coefficients C_L, C_D, which is the case for wings making use of a stabilized LEV such as delta wings (Polhamus 1966) and insects (Ellington *et al.* 1996; Dickinson *et al.* 1999). Note that it has been usually argued that LEV and leading-edge suction do not coexist (Polhamus 1966; Ramesh *et al.* 2014). In fact, the recent concept of the leading-edge suction parameter (LESP) is mainly based on this hypothesis, which was postulated by Ramesh *et al.* (2014) as a criterion for the formation of a LEV: an airfoil can sustain leading-edge suction up to a certain limit (depending on the geometry and R), and if the LESP exceeds this maximum value, leading-edge separation will occur (i.e. a LEV will form). Therefore, a plausible definition of the suction force coefficient C_S in terms of the computed lift and drag coefficients is

$$C_S = C_L \tan \alpha - \left(C_D - C_{D,f} \right), \tag{5.16}$$

where $C_{D,f}$ is the skin friction drag coefficient. Using the URANS computational results of $C_{L,s}$ and $C_{D,s}$, we use (5.16) to determine the suction force coefficient C_S, as shown in figure 5(*a*).

Figure 5(*a*) shows a large difference between $C_L \tan \alpha$ and C_D at small angles of attack, indicating a large suction force over this range. However, this difference attains a maximum at $\alpha = 15°$, supporting the LESP claim: there is a maximum suction force

928 A30-22

that can be sustained by an airfoil at a given R (Ramesh *et al.* 2014). Beyond this angle of attack, figure 5(*a*) shows that the suction force diminishes as the angle of attack increases in accordance with previous findings in literature (Usherwood & Ellington 2002; Dickson & Dickinson 2004; Yan *et al.* 2014). Moreover, at larger angles of attack (above 20°), indeed the behaviour of $C_L \tan \alpha$ is quite close to C_D with an almost constant shift ($C_{D,f}$), which indicates vanishing of the suction force. These results are quite plausible and intuitive.

Focusing on the change in the mean drag due to plunging, we normalize this change by the effect of kinematics (plunging amplitude) as it appears in (5.14): $H^2 k^2$. In particular, we denote the term between square brackets by $-\chi_T$, and call χ_T the thrust control parameter: if it is positive, it indicates drag reduction or thrust production; and if it is negative, it indicates drag increase. It simply represents the thrust-production capability due to plunging; if it is larger at condition A than condition B, it implies that more thrust would be produced at A than B when oscillating by the same effective-angle-of-attack amplitude: $A_{\alpha_{eff}} = \arctan Hk$. In fact, the actual thrust coefficient C_T would be given from χ_T through multiplying by $\tan^2 A_{\alpha_{eff}}/4$.

Normalizing (4.13) by $\rho U^2 b$, we obtain the following relation between C_S and C_L:

$$C_S = \frac{k_S}{4\pi^2} C_L^2, \tag{5.17}$$

which can be used to estimate the suction parameter k_S from the computed C_L and C_D, as shown in figure 5(*a*). Interestingly, the suction parameter increases beyond its potential-flow value 2π, although the suction force itself is less than its potential-flow counterpart $2\pi \sin^2 \alpha$. In fact, figure 5(*a*) implies that the parameter k_S actually varies with α; i.e. $k_S = k_S(\alpha)$. Taking this variation into account in our averaging analysis, we obtain more contributions to the thrust control parameter χ_T besides (5.14), due to the k_S-derivatives

$$\Delta \chi_T = \frac{1}{\pi^2} C_{L,s}(\alpha^*) \left[k_{hf} k_S' C_L' + k_S'' C_L/4 \right] |_{\alpha=\alpha^*} + O(\epsilon^3). \tag{5.18}$$

Equations (5.14), (5.18) imply that χ_T depends on the mean angle of attack α^*; that is, the ability to generate thrust from low-amplitude, high-frequency plunging depends on the mean angle of attack.

Figure 5(*b*) shows a comparison among several estimates of the χ_T-variation with the angle of attack: (i) the total (combined) χ_T from (5.14), (5.18), which considers $k_S = k_S(\alpha)$; (ii) the definition (5.14), ignoring the functional variation of k_S with α (i.e. no k_S-derivatives) in the averaging analysis; (iii) a no-suction solution: $k_S = 0$; and (iv) a full-suction solution considering a constant $k_S = 2\pi$. The difference between (i) and (ii) is clearly the effects of k_S-derivatives; the difference between (ii) and (iv) represents the departure of k_S from the ideal value 2π (mainly in the stall and post-stall regimes); the difference between (ii) and (iii) represents the contribution of suction force; and finally the no-suction solution represents the effect of the curvature $C_{L,s}''$: it is simply $-C_{L,s}'' \tan \alpha^*$. This comparison reveals some interesting points. First, at small angles of attack, $\chi_T > 0$, mainly due to suction effects; this is the classical thrust-production mechanism in the linear regime (Garrick 1937). Second, as the angle of attack increases towards stall, there is a strong effect of suction as implied from the small difference between the full-suction solution and the (5.14) definition. However, this strong effect of suction is negative, leading to an increased drag ($\chi_T < 0$) rather than thrust production. This behaviour is due to the weak slope $C_{L,s}'$ and strong negative curvature $C_{L,s}''$ of the lift curve near stall, leading to a positive coefficient of k_S in (5.14); i.e. a negative χ_T. In other words, while the suction

force is the main thrust generator in the linear regime, it has a negative effect in the stall regime; the no-suction solution is actually thrust producing in this regime (due to the negative curvature $C''_{L,s}$), as shown in figure 5(b). Having said that, it must be pointed out that the effect of k_S-derivatives is significant in this range because the suction force increases at a large rate near stall before dropping. Therefore, the net result still ensures a thrust-producing capability: $\chi_T > 0$. Computational validation below confirms these findings and shows a thrust-producing capability near stall: at angles of attack ($14°$) quite close to the stall angle ($15°$). Third, right after stall (the suction force stalls slightly after the lift), all the factors contribute in the same direction of a drag increase. The suction force collapses as shown in figure 5(a), which is also observed in the small difference between the no-suction solution and the (5.14) in figure 5(b). Moreover, this rapid decrease of the suction force results in a negative contribution of the k_S-derivatives: the total χ_T is considerably below the (5.14)-definition and the no-suction solution over this range, as shown in figure 5(b). As a result, the thrust-producing capability is annihilated; a huge rise in the mean drag coefficient occurs due to plunging in this range, which is validated below by computational simulations: URANS simulations show that the largest mean drag due to plunging with $k = 0.5$, $A_{\alpha_{eff}} = 5°$ over the range $0 \leqslant \alpha^* \leqslant 20°$ occurs at $\alpha^* = 16, 17°$, as will be shown in § 6 below. Finally, figure 5(b) interestingly shows a recovery of χ_T in the post-stall regime after the negative peak. This fact is also validated below; the URANS simulations indeed show a thrust production at $\alpha^* = 18°$ (see figure 14). The comparison in figure 5(b) implies that this recovery is due to the k_S-derivatives; (5.18) suggests that this behaviour is due to the negative slopes of k_S and C_L (the first term).

The effect of pitching on the drag dynamics can be studied in a similar way

$$
\bar{C}_D = C_{D,s}(\alpha^*) + \frac{A_\alpha^2}{4}\left[2\frac{C_{L,s}\tan\alpha + k_{hf}C'_{L,s}}{\cos^2\alpha} + k_{hf}C''_{L,s}\tan\alpha + \right.
$$
$$
- \frac{k_S}{2\pi^2}\left(k_{hf}C_{L,s}C''_{L,s} + k_{hf}^2 C'^2_{L,s} + k^2\left[k_{hf}k_{\dot\alpha}(k_{hf}k_{\dot\alpha} - 2\pi) + \pi^2\right]\right)
$$
$$
\left. - \frac{C_{L,s}}{\pi^2}\left(k_{hf}k'_S C'_{L,s} + k''_S C_{L,s}/4 \right)\right]_{\alpha=\alpha^*} + O(\epsilon^3). \tag{5.19}
$$

Equation (5.19) for the pitching effects on drag/thrust production shows similar terms to plunging effects in (5.14). However, unlike plunging, the effect of reduced frequency appears explicitly in the thrust control parameter χ_T mainly through rotational contributions (proportional to $k_{\dot\alpha}$). Therefore, there are non-zero kinematic effects on χ_T due to pitching, as shown in figure 6: the larger the reduced frequency k and the more backward the pitching axis (smaller $k_{\dot\alpha}$), the larger the thrust-producing capability (i.e. χ_T). However, these effects of kinematics are not observed in the post-stall regime where the suction force is diminished. Note that (5.19) implies that the k-effects are associated with suction (i.e. proportional to k_S). Another notable difference between plunging and pitching effects on thrust production is the well-known fact that, unlike plunging, pure pitching is thrust producing only beyond a certain threshold of frequency (Garrick 1937): figure 6 shows a drag rise over small α^* when pitching at $k = 1$ vs a slight thrust production when pitching at $k = 2$. The current results also indicate that the pitching thrust-production capability increases with the mean angle of attack up to stall. That is, pitching is significantly more efficient in thrust production near stall than at small angles of attack. Finally, it should be reported that the coupled pitching–plunging (low-amplitude, high-frequency) effects are of higher orders in ϵ than the individual effects.
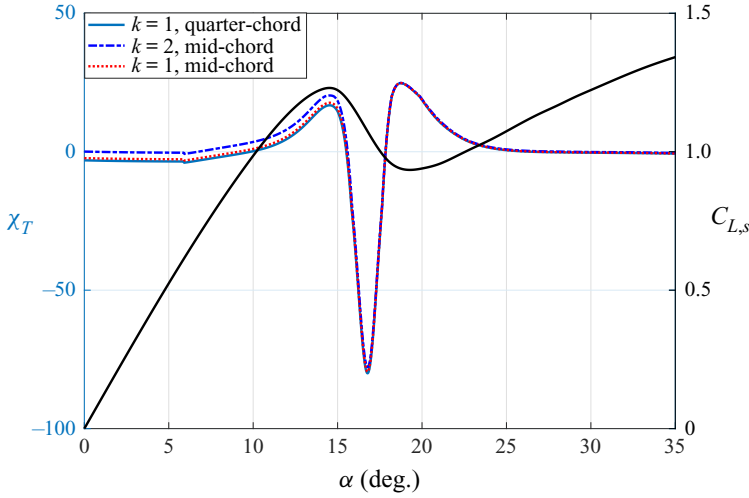
Figure 6. Variation of the thrust control parameter χ_T due to low-amplitude, high-frequency pitching with the mean angle of attack.

5.5. *Averaged separation*

Applying the averaging analysis above to the output variable Ψ_s describing the chord-normalized location x_s of the separation point, we obtain

$$\bar{x}_s = x_0(\alpha^*) + \frac{k^2}{4}x_0''(\alpha^*)\left[H^2 + A_\alpha^2 \hat{\tau}_2^2\right] + O(\epsilon^4), \tag{5.20}$$

where $x_0(\alpha)$ is the steady separation point and $\hat{\tau}_2 = U\tau_2/b$ with τ_2 being the Goman–Khrabrov delay (Goman & Khrabrov 1994), as defined in (4.14). The Kirchhoff model, which relates the steady lift coefficient $C_{L,s}$ to the separation point x_0, as given in (4.15), can be used to estimate the variation of the separation point with the angle of attack from a given steady lift curve

$$x_0(\alpha) = \left(2\sqrt{\frac{C_{L,s}(\alpha)}{2\pi \sin \alpha}} - 1\right)^2. \tag{5.21}$$

If the flow is fully attached (i.e. $x_0 = 1$), then Kirchhoff's model results in the classical potential-flow lift $C_{L,s} = 2\pi \sin \alpha$; the larger the deviation of $C_{L,s}$ from this classical relation, the smaller x_0 (i.e. earlier separation).

Using the URANS $C_{L,s}$ computations, we use the Kirchhoff model (5.21) to estimate the variation of separation point x_0 with the angle of attack, as shown in figure 7. The figure also shows the averaged unsteady separation point $\bar{x}_s$ due to plunging with $A_{eff} = 5°$. The current analysis implies that plunging promotes separation in the pre-stall regime, which is intuitively expected, but provides a significant delay of separation if performed in the post-stall regime near the trough of the $C_{L,s}$-α curve.

5.6. *Added-mass effects*

The above analysis did not reveal any added-mass effects up to $O(\epsilon^2)$ because of the additional lag τ_v; only higher-order effects will be captured. However, if such a lag is relaxed ($\tau_v = 0$), the analysis will reveal some important added-mass effects. For example,
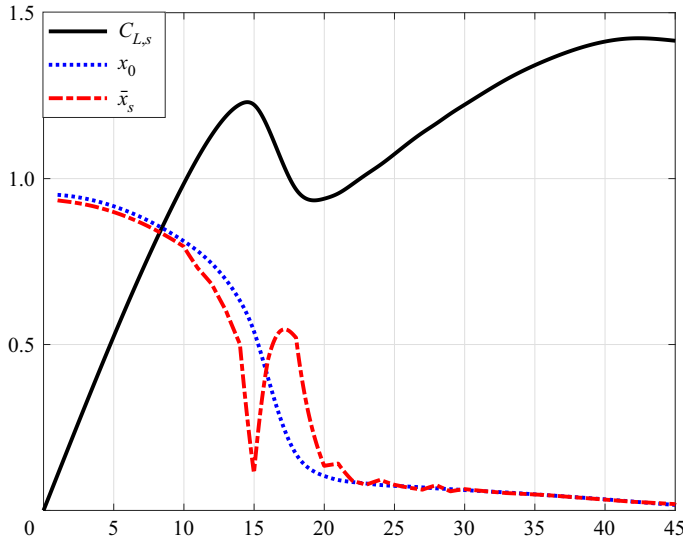
Figure 7. Variation of the steady separation point x_0 with the mean angle of attack along with the mean unsteady separation point due to plunging with $A_{eff} = 5°$.

pure pitching is found to provide lift enhancement only when the pitch axis is ahead of the mid-chord ($a < 0$), while a combined pitching–plunging motion can result in lift enhancement independent of the hinge location

$$\Delta_{m_v} \bar{C}_L = \frac{\pi}{4} \mu_v k^2 A_\alpha [H \sin 2\alpha^* \sin \phi - 2a A_\alpha \sin \alpha^*], \qquad (5.22)$$

where Δ_{m_v} denotes an added-mass contribution, μ_v is the mass ratio ($\mu_v = m_v/\pi\rho b^2$: added-mass normalized by its potential-flow value) and ϕ is the phase difference between the two harmonic motions, as defined in (5.1a,b). It should be noted that this lift enhancement mechanism due to added mass may not be well known; it is actually a non-intuitive mechanism in the sense that it is purely inertial, so one might think that purely harmonic inertial loads may not have net/averaged effects. However, the current geometric nonlinearities in α promoted such a mechanism. Definitely, it cannot be captured by a purely linear analysis.

Similarly, pure pitching is found to produce thrust when the pitch axis is ahead of the mid-chord ($a < 0$), while a combined pitching–plunging motion can be thrust producing at any hinge location if the relative phase is set appropriately

$$\Delta_{m_v} \bar{C}_D = -\frac{\pi}{2} \mu_v k^2 A_\alpha [H \cos^2 \alpha^* \sin \phi - a A_\alpha \cos \alpha^*]. \qquad (5.23)$$

Unlike the lift enhancement mechanism due to added mass, this thrust-production mechanism is well known (Garrick 1937). In fact, the second term reduces to Garrick's potential-flow result on the added-mass contribution when taking the limit to small angles of attack ($\cos \alpha^* \to 1$) and considering potential-flow characteristics ($\mu_v = 1$). As shown in figure 8, the added-mass contributions (when pitching at the quarter-chord) may provide significant thrust particularly at high frequencies (it varies quadratically with k). Finally, it should be reported that no net added-mass effects due to pure plunging are observed.
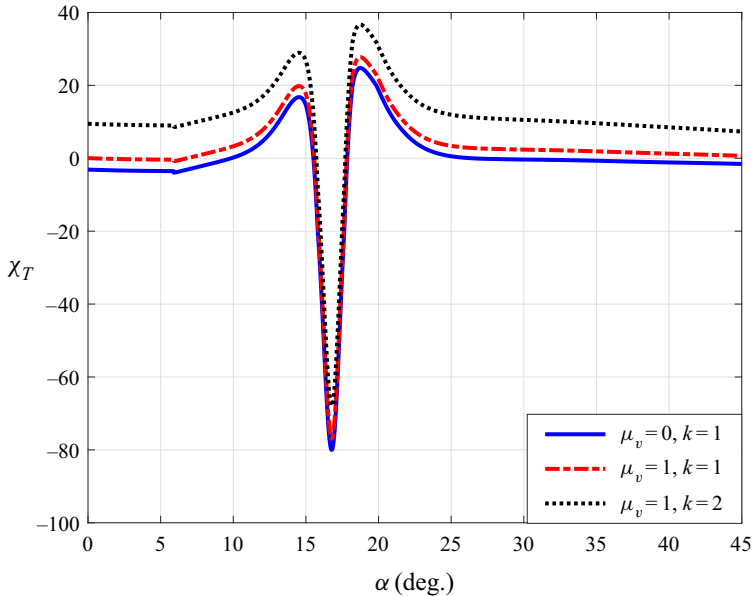
928 A30-26

Figure 8. Added-mass effects on the thrust control parameter χ_T due to pitching at the quarter-chord at different reduced frequencies.

6. Computational validation and distillation of the flow physics

In this section we aim to validate some of the theoretical results obtained in the previous section and illustrate their underlying physics. In particular, we focus on plunging effects on lift enhancement/deficiency and thrust production. For this purpose, we solve the URANS equations on a harmonically plunging NACA 0012 airfoil at $R = 500$ K. We should acknowledge that URANS may not be the most appropriate solver for validation in the critical and rich regimes of stall and post-stall as ensemble averaging may fail to capture chaotic vortex interactions (Lesieur, Métais & Comte 2005, pp. 19–20). However, there are several factors that may justify such a choice. First, the need to perform many simulations at this large Reynolds number may preclude a more accurate and detailed simulation (e.g. DNS or LES). Second, the focus on a two-dimensional case study may mitigate the issue as it obviates the three-dimensional mechanisms (e.g. vortex stretching) that promote energy transfer between small and large scales. Third, the focus on global (integrated) quantities such as lift and drag forces, particularly their cycle-averaged values, may also justify such a choice. Finally, perhaps most importantly, we do not seek a quantitative validation; in fact, the above theoretical analysis is not meant to provide quantitative results, but qualitative behaviours as discussed previously. Therefore, when the theoretical analysis predicts lift enhancement in some region, we validate such a qualitative behaviour without scrupulously investigating how much enhancement is attained.

In fact, it may be prudent here to point out that the sought validation of the theoretical results, obtained above, may actually be independent of the solver type. To illustrate this point, recall that the conducted theoretical analysis derives averaged values of unsteady quantities (e.g. C_L, C_D) from their steady behaviours. It is precisely this relation that is being validated. For example, the above theoretical analysis revealed an unsteady lift enhancement when oscillating over regions of positive curvature of the steady lift curve. Since the same solver is used in computing both the steady and unsteady characteristics,

it may make the choice of the solver type a subtle point rather than a core one. Nevertheless, the solver choice would certainly affect our attempt to explain the underlying physics behind such a result.

6.1. *Computational set-up*

All simulations are performed using the ANSYS FLUENT commercial package, while meshes are generated using the ICEM CFD software. To handle the airfoil plunging motion, we split the mesh domain (with a C-grid topology) into two different zones: an inner moving circular zone and a static outer one. The inner zone moves with the airfoil as a rigid body, while the outer deforms (using the Dynamic Mesh feature in FLUENT) to accommodate this motion. The inlet semicircle has a 15 chord radius, measured from the quarter chord, while the downstream extends to 30 chords. The inner circular zone radius is 7 chords. The meshes of the two zones are generated using Multi Blocking in ICEM CFD to obtain a two-dimensional quad structured mesh. A grid independence study is performed to reach a final mesh of 102 000 elements with 420 over a sharp trailing edged airfoil, 200 over each of the semi-circle inlet, outlet and upper and lower edges. A boundary layer mesh treatment is implemented with a first layer height of $h = 2.15$ e-5 chord, which is half of the value estimated from Schlichting *et al.* (1960); this choice ensured $y^+ < 1$ for proper turbulence modelling.

The simulations are performed using the pressure-based solver. Turbulence is modelled using the Menter shear stress transport k-ω SST two-equation complete model (Menter 1994). The model possesses a good capability in predicting separation, which is important for the current study. Moreover, it can handle high pressure gradients in near-wall viscous layers (Wilcox 1998; Pope 2000; Wilcox 2008). The upstream semi-circle and upper and lower edges are set as velocity inlets; and the downstream edge is set as a pressure outlet. Finally, a no-slip wall is set for the airfoil surface. A sliding mesh interface is used between the moving and deforming zone. The airfoil, inner zone and interface edge motion has a rigid body user defined function written to implement the motion. The smoothing dynamic mesh method is used to deform the mesh as springs; and re-meshing is not used because the motion amplitude is relatively small compared with the domain size. The pressure–velocity coupled scheme is adopted. The second-order upwind scheme is selected for spatial discretization and a second-order dual time stepping implicit scheme is adopted for temporal integration with a time step adjusted to ensure 430 steps per motion cycle; and 20 iterations per time step were adopted to ensure convergence in the inlet–outlet net-mass residuals. Finally, simulations are performed until periodicity of the lift coefficient is observed.

6.2. *Lift enhancement*

The above theoretical analysis, (5.13), revealed the role of the curvature $C_{L,s}''$ of the steady $C_{L,s}$-α curve in controlling enhancement (or deficiency) in the mean lift due to low-amplitude, high-frequency oscillations. To validate this finding, we first constructed the steady $C_{L,s}$-α curve using the URANS computational set-up discussed above, as shown in figure 9(a). Below $\alpha = 16°$, no vortex shedding is observed at this Reynolds number. For $\alpha > 16°$, the mean values of the steady lift curve are considered for analysis, after smoothing by cubic splines. According to figure 9(a), the curvature is most negative around the peak at $\alpha = 15°$ and is most positive around the trough at $\alpha = 20°$. So, these two points may be good candidates to test the hypothesis by performing plunging oscillations around these two mean angles of attack with a high frequency ($k = O(1)$) and low
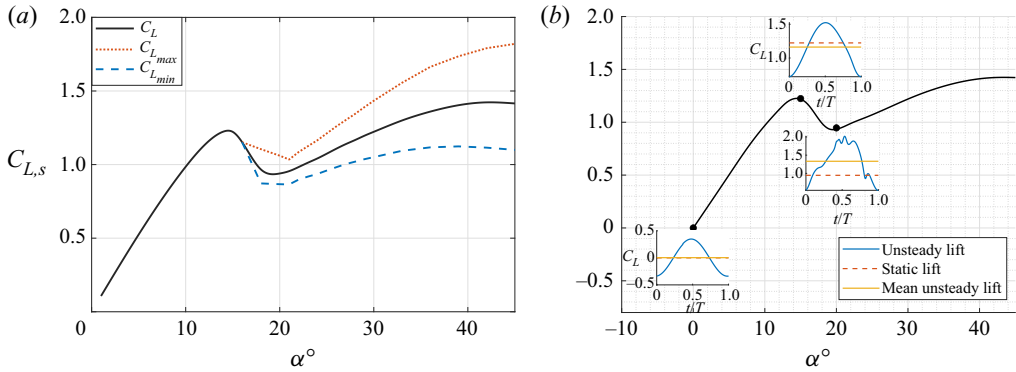
Figure 9. URANS steady $C_{L,s}$-α curve for NACA 0012 at $R = 500$ K along with plunging simulations around $\alpha^* = 0, 15, 20°$ with $k = 0.5$ and $A_{\alpha_{eff}} = \arctan HK = 5°$. (a) $C_{L,s}$-α^* curve. (b) Lift enhancement/deficiency.

amplitude ($H = O(\epsilon)$). There is also another limitation on the plunging amplitude so that the effective angle of attack $\alpha_{eff} = \alpha^* \pm \arctan Hk$ stays within the designated range (of signed curvature). Therefore, we performed plunging simulations around $\alpha^* = 0, 15, 20°$ with $k = 0.5$ and $A_{\alpha_{eff}} = \arctan Hk = 5°$, as shown in figure 9. The figure shows 40.6 % enhancement in the mean lift coefficient when plunging around $\alpha^* = 20°$ (i.e. $C''_{L,s} > 0$); 5 % decrease in the mean lift coefficient when plunging around $\alpha^* = 15°$ (i.e. $C''_{L,s} < 0$); and almost no change in the mean lift coefficient when plunging around $\alpha^* = 0°$ (i.e. $C''_{L,s} = 0$), which is in accordance with the theoretical result from the combined geometric-control-averaging analysis. Indeed, geometric-control theory provides heuristic tools for discovery of nonlinear force-generation and stabilization mechanisms.

It may be interesting to investigate why this happens. Why does plunging around $\alpha^* = 20°$ provide such a significant lift enhancement while plunging around $\alpha^* = 15°$ with the same amplitude and frequency results in a lift deficiency instead? To investigate this point, we show in figure 10 the time history of the unsteady lift coefficient C_L along with the quasi-steady one $C_{L,s}(\alpha_{eff})$ for the two cases, and also show snapshots of the vorticity contours over the cycle for the two cases in figures 11, 13. The following list provides a chronological description of the airfoil motion during the cycle:

(i) (*a*) Start at the mid-stroke (i.e. maximum $\dot{h}$ with $\alpha_{\text{eff}} = \alpha^* - A_{\alpha_{eff}}$).
(ii) (*a*)–(*c*) Upward deceleration: until the airfoil reaches the top dead centre after (*c*) at $t/T = 0.25$.
(iii) (*c*)–(*e*) Downward acceleration: until the airfoil reaches the mid-stroke point again after (*e*) at $t/T = 0.5$.
(iv) (*e*)–(*g*) Downward deceleration: until the airfoil reaches the bottom dead centre after (*g*) at $t/T = 0.75$.
(v) (*g*)–(*i*) Upward acceleration: until the airfoil reaches the mid-stroke point after (*i*) at $t/T = 1.0$.

Figures 11, 13 show that, as the airfoil decelerates upward between (*a*–*c*), the flow reattaches. During this phase, there is a trailing-edge vortex (TEV) in the two cases, although significantly stronger in the 20° case. This TEV explains why the unsteady lift is less than its quasi-steady counterpart during this phase, as shown in figure 10; this difference is significantly larger in the 20° case. It is the classical Wagner wake deficiency effect (Wagner 1925). As the airfoil moves upward, the TEV gets fainter
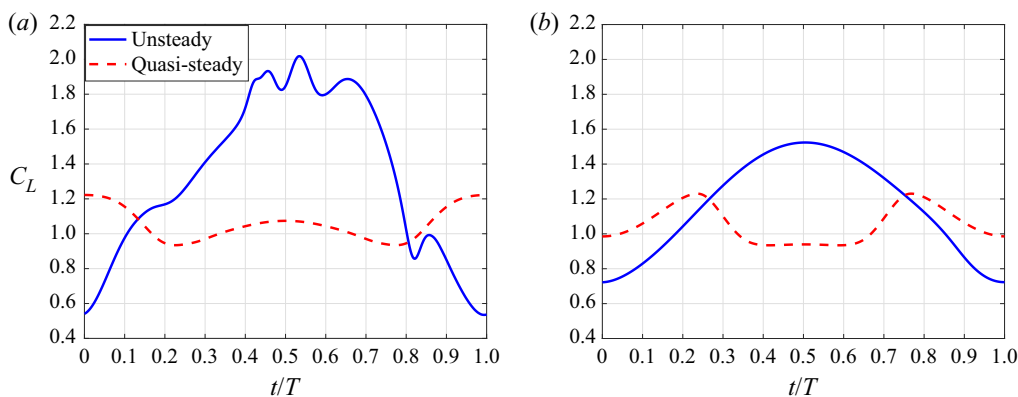
Figure 10. Variations of the unsteady lift coefficients along with the quasi-steady ones over the plunging cycles around $\alpha^* = 15, 20°$ with $k = 0.5$ and $A_{\alpha_{eff}} = 5°$. (a) $\alpha^* = 20°$ and (b) $\alpha^* = 15°$.
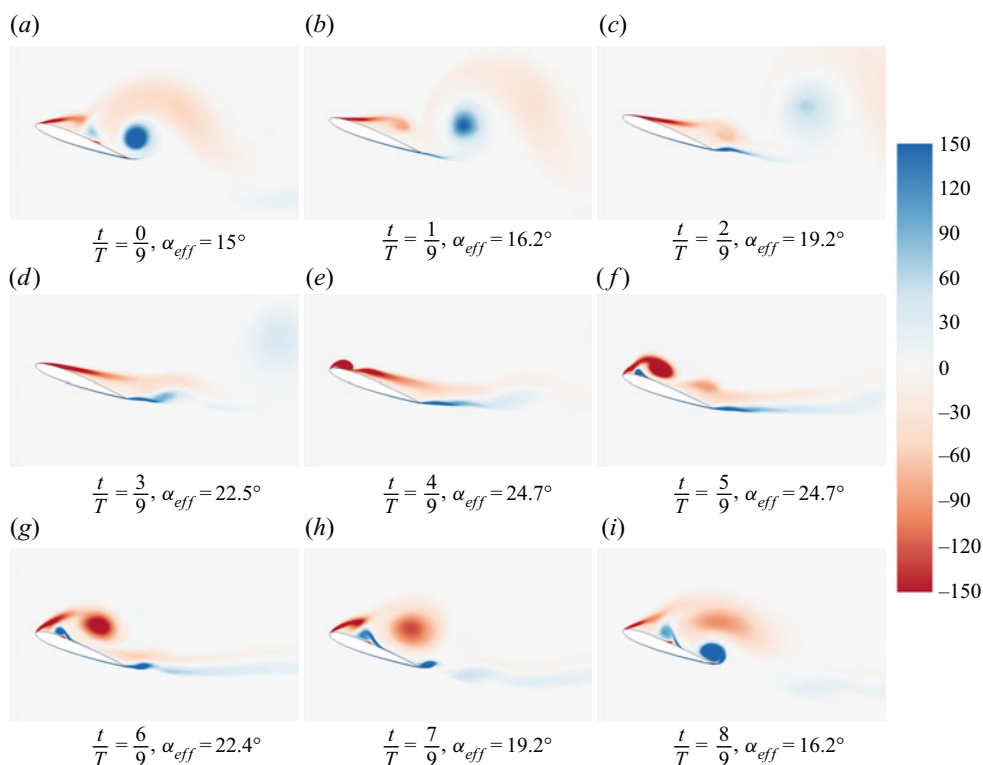

Figure 11. Vorticity contours over the plunging cycle around $\alpha^* = 20°$ with $k = 0.5$ and $A_{\alpha_{eff}} = 5°$.

and fainter, consequently, the unsteady lift gets closer to the quasi-steady behaviour. It increases at a faster rate in the 20° case. In this case, at some early moment in the downstroke – between (d,e) at $t/T \simeq 0.4$ – a LEV forms, as shown in figure 11. It then grows and moves relatively slowly; it remains over the airfoil for a considerable part of the cycle (approximately a third of the cycle). Therefore, this attached LEV explains the lift enhancement in the 20° case: the C_L reaches almost double the quasi-steady value

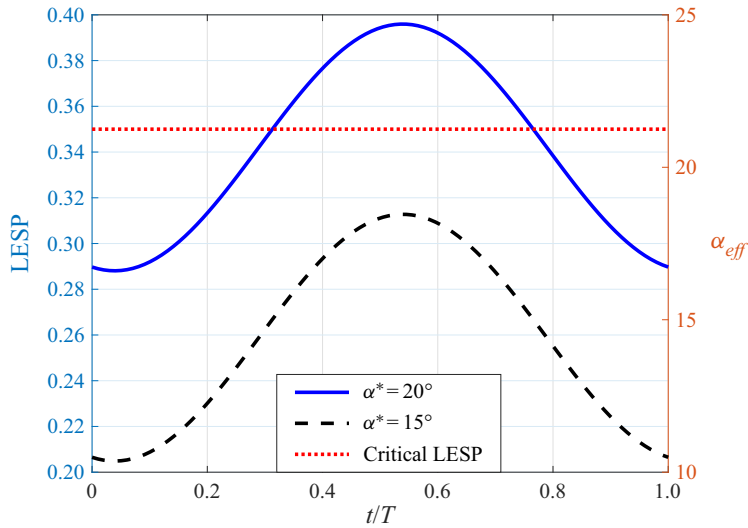**928** A30-30

Figure 12. LESP variation over the plunging cycle in the two cases of $\alpha^* = 15, 20°$ with $k = 0.5$ and $A_{\alpha_{eff}} = 5°$ along with the critical LESP for NACA 0012 at $R = 500$ K.

specifically during the period ($t/T = 0.4$–0.7) where the LEV is attached to the airfoil. On the other hand, this strong LEV is not observed in the 15° case, as shown in figure 13, which answers the posed question. It should be noted that at these large angles of attack (15° or 20°), whether static or dynamic, there is a continuous flow of small-scale shear layers separating from the leading edge. However, the current URANS simulation captures only the large coherent structures.

We then pose another question: Why does a strong LEV form in the 20° case and not in the 15° case? Since the question here is about the formation of a LEV as a large coherent structure (not leading-edge separation in general), the LESP concept (Ramesh *et al.* 2014) may be a convenient tool in this case. While the LESP concept was introduced for low Reynolds number applications, there are some recent efforts to extend it to high Reynolds number flows (Narsipur *et al.* 2016). Unlike the low Reynolds number case, the critical LESP has some kinematic dependence at high Reynolds numbers. In particular, it increases with k until it reaches a maximum value around $k = 0.5$. It is found that the critical LESP for NACA 0012 at a relatively high k ($\simeq 0.5$) ranges from 0.32 at $R = 30\,000$ up to 0.5 at $R = 3\,000\,000$ (Narsipur *et al.* 2016). Performing a simple interpolation between the two values, we postulate a 0.35 critical LESP for the current case of $R = 500\,000$. Moreover, for pure plunging, one can show that the LESP may be approximated as (Ramesh 2020)

$$\text{LESP}(t) = \sin \alpha^* + \frac{\dot{h}(t)}{U} C(k), \quad (6.1)$$

where $C(k)$ is Theodorsen's lift transfer function. Figure 12 shows the LESP variation over the plunging cycle in the two cases of $\alpha^* = 15, 20°$ with $k = 0.5$ and $A_{\alpha_{eff}} = 5°$ along with the LESP critical value (0.35). The figure clearly shows that the LESP in the 20° case exceeds the critical value around $t/T \simeq 0.31$, indicating the formation of a LEV around this instant, which matches the vorticity snapshots shown in figure 11. On the other hand, the LESP (equivalently the unsteady effective angle of attack) in the 15° is not strong enough to initiate a LEV.
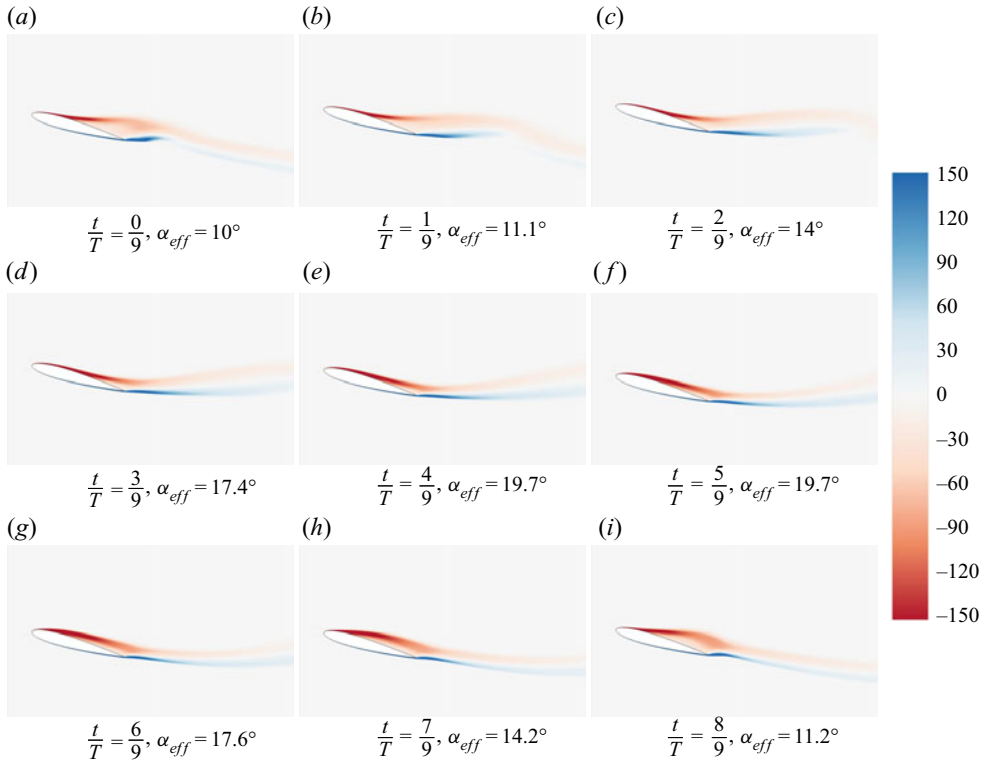
(a) $\dfrac{t}{T} = \dfrac{0}{9}, \alpha_{eff} = 10°$

(b) $\dfrac{t}{T} = \dfrac{1}{9}, \alpha_{eff} = 11.1°$

(c) $\dfrac{t}{T} = \dfrac{2}{9}, \alpha_{eff} = 14°$

(d) $\dfrac{t}{T} = \dfrac{3}{9}, \alpha_{eff} = 17.4°$

(e) $\dfrac{t}{T} = \dfrac{4}{9}, \alpha_{eff} = 19.7°$

(f) $\dfrac{t}{T} = \dfrac{5}{9}, \alpha_{eff} = 19.7°$

(g) $\dfrac{t}{T} = \dfrac{6}{9}, \alpha_{eff} = 17.6°$

(h) $\dfrac{t}{T} = \dfrac{7}{9}, \alpha_{eff} = 14.2°$

(i) $\dfrac{t}{T} = \dfrac{8}{9}, \alpha_{eff} = 11.2°$

Figure 13. Vorticity contours over the plunging cycle around $\alpha^* = 15°$ with $k = 0.5$ and $A_{\alpha_{eff}} = 5°$.

6.3. *Drag reduction/thrust generation*

The above theoretical analysis, (5.14), (5.18) and figure 5(*b*), revealed an interesting behaviour of the thrust control parameter χ_T with the mean angle of attack α^*. It shows a positive χ_T (i.e. an ability to generate thrust from plunging oscillations) up to the stall angle of attack beyond which there is a significant rise in the mean drag coefficient due to the collapse of the suction force. Moreover, the thrust-producing capability is recovered when increasing the mean angle of attack beyond the stall regime. To validate these findings, we performed plunging simulations at several mean angles of attack ($\alpha^* = 0°$, $12°$, $14°$, $15°$, $16°$, $17°$, $18°$) with $k = 0.5$. For each simulation, we compute the mean drag coefficient $\bar{C}_D$ and use it to estimate the thrust control parameter χ_T as

$$\chi_T(\alpha^*) = \frac{\bar{C}_D - C_{D,s}(\alpha^*)}{H^2 k^2/4}, \tag{6.2}$$

where $C_{D,s}(\alpha^*)$ is the mean drag coefficient at a static angle of attack equal to α^*. Although we do not seek a quantitative validation, the comparison between theoretical predictions (5.14), (5.18) and the URANS computations, shown in figure 14, is encouraging – to capture the drag dynamics in the critical stall regime with such an accuracy using the present simple modelling and analysis is more than satisfactory.
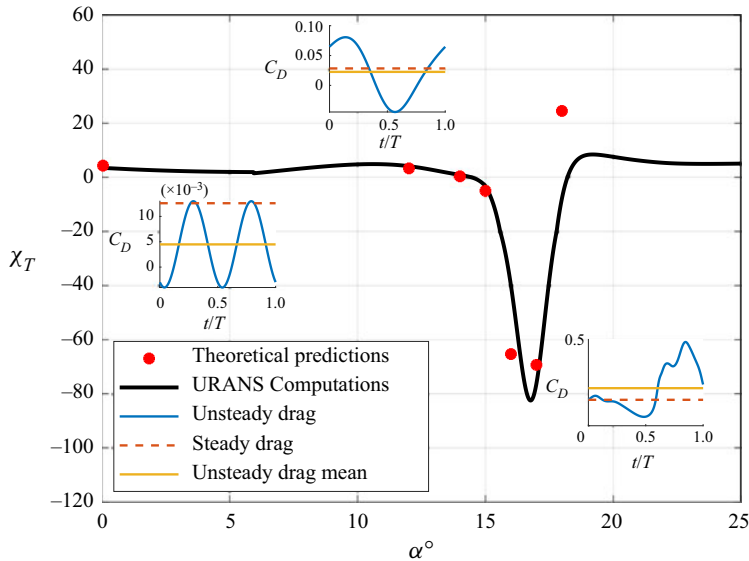
Figure 14. Validation of the thrust control parameter χ_T due to plunging against URANS computational simulations of a plunging NACA 0012 with $k = 0.5$ at $R = 500$ K.

7. Discussion

Before concluding this paper, it may be judicious to discuss how this simple theoretical modelling and analysis could capture such nonlinear dynamical behaviours of the lift and drag near stall. There are several points worthy of discussion in this regard. First, the main – perhaps the only – modelling assumption in this work is that the lift output is dictated by the quasi-steady circulation (or lift) through a linear dynamical system. This assumption is not far from truth even in the stall regime. What the first part of this assumption entails is that when the airfoil experiences a step change in the angle of attack, the lift goes through some transient response, but finally settles on the steady value. If there is no periodic vortex shedding, this behaviour is indeed correct; the lift attains an equilibrium point dictated by the steady behaviour. Even with a periodic vortex shedding, the behaviour still holds, although the lift attains a periodic orbit instead. Nevertheless, such oscillatory behaviour is captured in the stability (eigenvalues) of the linear dynamical system between the quasi-steady circulation and the unsteady lift: stable in the former case of no vortex shedding and unstable (or critically stable) in the latter case of periodic vortex shedding. Therefore, the lift output is indeed governed by the quasi-steady circulation (or lift). The only remaining issue would be questioning the linearity of such a dynamical system. To discuss this point, we recall that there are two types of nonlinearities: nonlinearity of the input–output map (e.g. a nonlinear relation between α as an input and C_L as an output), and nonlinearity of the underlying dynamical system (i.e. nonlinearity in the states constituting such a dynamical system). The former is indeed captured in the proposed model. As for the latter, if the system is feedback linearizable, then there exists a nonlinear transformation that renders the dynamical system a linear form. Therefore, we assume to work directly with the transformed states – since the state variables are arbitrary in the present formulation. Moreover, even if such a transformation does not exist (i.e. the system is not feedback linearizable), the nonlinear system may still be represented by a linear form in a larger space – by adding more state (see the work

of Sassano & Astolfi 2016). In other words, it may have a finite-dimensional Koopman invariant subspace (Brunton *et al.* 2016*a*). Since the order of the linear dynamical system relating quasi-steady circulation to unsteady lift in our ROM is arbitrary, it implies that our formulation includes all of the above scenarios. Finally, even if the lift dynamics is different from all of the above cases, confining our analysis to small amplitudes might justify the linearity assumption, stressing that we assume linearity between quasi-steady circulation (or lift) and unsteady lift – not between lift and angle of attack. Indeed, the angle of attack is a state variable and it appears nonlinearly in the developed ROM. So, in conclusion, the modelling strategy is wide enough to allow for unconventional lift mechanisms and an arbitrary lift dynamics. In fact, it obviates assuming a specific form and leaves it open. After all, it is a high-fidelity-informed theoretical model; the model is driven by high-fidelity steady lift and drag characteristics.

The second point is regarding the combined geometric-control-averaging analysis. It should be noted that the averaging theorem guarantees that the response $x(t)$ of the time-periodic system and that of the averaged system are close only over a finite time horizon: $x(t) - \bar{x}(t) = O(\epsilon) \ \forall t \in [0, \sigma/\epsilon]$ (see Appendix A), which cannot be used to draw conclusions about the steady-state mean values of the unsteady lift and drag forces from the averaged system. We can only guarantee closeness between $x(t)$ and $\bar{x}(t)$ over an infinite horizon if the averaged dynamics has an exponentially stable fixed point. Only in this case, we can draw conclusions about the steady-state mean values of lift and drag from equilibria of the averaged dynamics. However, near stall, where we have periodic vortex shedding, the lift dynamics is essentially unstable or critically stable (eigenvalues on the imaginary axis), so we certainly lose exponential stability. This issue forms an impasse against the goal of the proposed analysis. However, luckily, when the unstable lift dynamics experiences periodic forcing with high enough frequency – and amplitudes (of the acceleration inputs) are also scaled with frequency – there is a strong chance for stabilization: vibrational stabilization (Meerkov 1980; Baillieul & Lehman 1996; Sarychev 2001; Taha *et al.* 2015*a*; Tahmasian & Woolsey 2017; Hassan & Taha 2019; Maggia *et al.* 2019; Taha *et al.* 2020). As a result, the lift natural oscillations will be suppressed; lift will oscillate at the forcing frequency. This behaviour is exactly the lock-in phenomenon (Karniadakis & Triantafyllou 1989; Young & Lai 2007). In other words, the vortex lock-in phenomenon is nothing but a vibrational stabilization of the lift dynamics. In this case where the averaged dynamics is stabilized, the proposed averaging analysis is conclusive. Therefore, the proposed geometric-control-averaging analysis is mainly valid when lock-in occurs.

Figure 15 shows the spectrum of the unsteady lift due to plunging around 20° with $k = 0.5$ and $A_{\alpha_{eff}} = 5°$. It also shows the spectrum of the lift variations at a static $\alpha = 20°$ (i.e. due to shedding). The shedding frequency is not present at all in the unsteady lift due to plunging: only the forcing frequency and its harmonics. Clearly, the plunging motion suppressed the natural vortex shedding, leading to lock-in. Finally, it may be important to point out that the order n and the nature of the states x_c constituting the linear dynamical system between the quasi-steady circulation Γ_0 and the circulatory lift L_C were irrelevant in this particular averaging analysis; the resulting averaged responses in (5.13), (5.14), (5.19) and (5.20) were found to be independent of n and the entries of A, B, C and D defining the x_c-dynamics; only the high-frequency gain k_{hf} was important. Since the focus was only on the steady-state-averaged output behaviour due to high-frequency input oscillations, the transient response – which is dictated by n and the x_c-dynamics – is irrelevant as long as it is exponentially stable as discussed above. It is then intuitively expected to observe the importance of the high-frequency gain k_{hf}. However, if some other nonlinear analysis is pursued, n and x_c-dynamics may play an instrumental role.
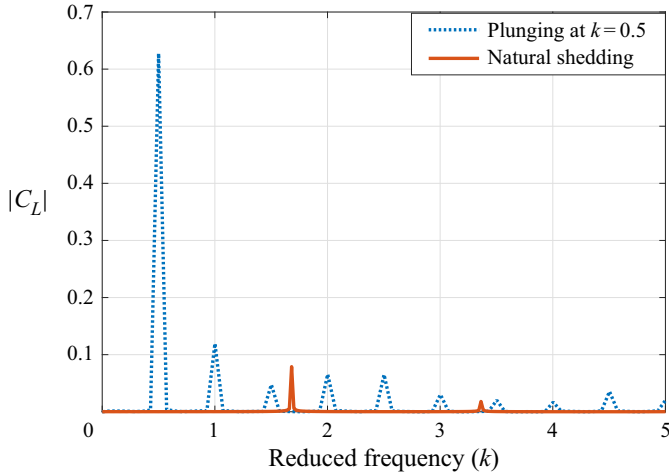
Figure 15. Frequency spectrum of the unsteady lift due to plunging around $20°$ with $k = 0.5$ and $A_{\alpha_{eff}} = 5°$, along with spectrum of the lift on the static airfoil at the same angle of attack.

For example, if one wishes to capture resonance effects between forcing and natural shedding, which may lead to interesting lift and thrust enhancement mechanisms, one must identify the $\boldsymbol{x}_c$-dynamics from computational simulations of the unsteady lift response at static angles of attack. In particular, the variations of the eigenvalues with the angle of attack must be incorporated. Then, a nonlinear systems analysis tool such as the method of multiple scales (Nayfeh 1973; Nayfeh & Mook 1979; Nayfeh & Balachandran 2004) may capture such a resonance effect.

8. Conclusion

This paper represents one of the first attempts to apply differential-geometric-control theory directly to an unsteady fluid dynamic system. We started by showing how geometric-control theory can be useful for a fluid dynamicist in (i) exploiting nonlinear interactions between control inputs to generate forces (or motion) in unactuated directions; (ii) suggesting symmetry-breaking mechanisms via high-frequency oscillatory control; and (iii) vibrational stabilization: stabilization via high-frequency oscillatory control. However, geometric-control theory – similar to typical nonlinear systems analysis tools – stipulates special forms for the dynamical system under study. Clearly, direct application of the theory to Navier–Stokes equations is not possible, hence the need for reduced-order modelling. The sought ROM must be (*a*) dynamical/unsteady (in the form of a differential equation), (*b*) nonlinear – the theory thrives on nonlinearities and (*c*) analytical; we do not seek an efficient simulation tool – rather, an analytical model to perform an analytical study (symbolic computations). It is found that none of the standard reduced-order modelling techniques available in the literature (e.g. POD, BPOD, ERA, DMD, EDMD, Volterra, neural networks, ...) can satisfy these essential requirements to enable true nonlinear analysis of a fluid dynamic system. In this paper, we overcome this hurdle by adopting a physics-based (phenomenological) modelling approach. We developed a geometric-control oriented ROM for the unsteady aerodynamics of a pitching–plunging wing that is (i) rich enough to capture the main physical aspects (e.g. nonlinearity of the flow dynamics at large angles of attack and high frequencies) and (ii) efficient and compact enough to be amenable to the analytic tools of geometric nonlinear control theory.

The analytical ROM of the unsteady lift and drag forces is informed by high-fidelity simulations at static angles of attack.

Applying geometric control and averaging analysis to the developed ROM, several interesting lift and drag mechanisms are revealed for low-amplitude, high-frequency oscillations. First, the curvature of the steady lift curve at the mean angle of attack controls lift enhancement/deficiency: the mean lift coefficient will increase when oscillating around regions of positive curvature (near the trough in the post-stall regime) and decrease when oscillating around regions of negative curvature (near the peak in the stall regime). Validation using URANS is in a good agreement with this theoretical finding, confirming that geometric-control theory is a heuristic tool for discovery. While the proposed theoretical analysis may not provide quantitative predictions, it points to regions of interesting mechanisms where one can perform higher-fidelity simulations to study the underlying physics. The URANS simulations revealed a strong attached LEV when oscillating around the trough of the lift curve, which does not form when oscillating around the peak. Hence, it explains the reason behind lift enhancement in the former case. The LESP concept confirms that the kinematics in this case (around the trough; i.e. larger values of the effective angle of attack) are strong enough to make the LESP exceed its critical value for this airfoil at the designated Reynolds number (500 K), explaining the formation of a LEV – in contrast to the former case (around the peak; i.e. smaller values of the effective angle of attack). The analysis also revealed a nonlinear lift enhancement mechanism due to added-mass effects that is not well documented in literature.

As for the drag/thrust, the current analysis captured the classical thrust production mechanism due to suction in the linear regime. In addition, it showed a huge drop in the suction force immediately after lift stall, which annihilated the thrust-production capability due to low-amplitude, high-frequency oscillations; there is a huge rise in the mean drag over this regime. Interestingly, the thrust-production capability is recovered in the post-stall regime. These behaviours are validated using URANS simulations; in fact, the validation shows a good quantitative agreement between computational simulations and theoretical predictions in this regard.

Author ORCIDs.
- Haithem E. Taha https://orcid.org/0000-0002-9242-2045;
- Laura Pla Olea https://orcid.org/0000-0002-9518-8055;
- Nabil Khalifa https://orcid.org/0000-0002-5541-2788;
- Cody Gonzalez https://orcid.org/0000-0003-3158-4304;
- Amir S. Rezaei https://orcid.org/0000-0003-3838-5607.

Author contributions. H.E.T. and L.P.O. developed the reduced-order model and performed theoretical analysis; N.K. performed computational simulations, C.G. and A.S.R. provided guidance in computational simulations and insight into the underlying physics; H.E.T. wrote the draft of the manuscript; and all authors contributed in refining it.

Appendix A. Formal averaging techniques

A.1. *The averaging theorem*

THEOREM A.1. *Consider the nonlinear, time-periodic (NLTP) system*

$$\dot{x}(t) = \epsilon X(x(t), t), \tag{A1}$$

where ϵ is a small perturbation scaling parameter, and X is a T-periodic vector field in t. The averaged dynamical system corresponding to (A1) is then written as

$$\dot{\bar{x}}(t) = \epsilon \bar{X}(\bar{x}(t)), \tag{A2}$$

where $\bar{X}(\bar{x}(t)) = (1/T) \int_0^T X(x(t), \tau) \, d\tau$. According to the averaging theorem (Khalil 2002; Sanders et al. 2007):

    (i) *If $x(0) - \bar{x}(0) = O(\epsilon)$, then there exist $\sigma > 0$ and $\epsilon^* > 0$ such that $x(t) - \bar{x}(t) = O(\epsilon) \; \forall t \in [0, \sigma/\epsilon]$ and $\forall \epsilon \in [0, \epsilon^*]$.*

    (ii) *If x^* is an exponentially stable equilibrium point of (A2) and if $\|x(0) - x^*\| < r$ for some $r > 0$, then $x(t) - \bar{x}(t) = O(\epsilon) \; \forall t > 0$ and $\forall \epsilon \in [0, \epsilon^*]$. Moreover, the system (A1) has a unique, exponentially stable, T-periodic solution $x_T(t)$ with the property $\|x_T(t) - x^*\| \leqslant \kappa \epsilon$ for some κ.*

Thus, the averaging theorem allows conversion of a non-autonomous system (time varying) into an autonomous (time-invariant) system. As such, if the equilibrium state of the NLTP system is represented by a periodic orbit $x_T(t)$, it reduces to a fixed point x^* of the averaged dynamics. Moreover, if this fixed point is stable, the averaging theorem will guarantee that the periodic response of the NLTP system is orbiting in close proximity to such a point. Hence, one can draw conclusions for the original NLTP system by analysing the simpler (time-invariant) averaged dynamics.

The main issue here is that the unsteady aerodynamic system (5.3) is not directly amenable to the averaging theorem above; it is not exactly in the form (A1). Specifically, it is not a weakly forced system whose vector field is scaled by ϵ (see a full discussion on this issue in the work of Maggia *et al.* 2019). Rather, it is forced by high-amplitude, high-frequency, periodic forcing. Note that while the airfoil oscillatory motion (α, h) is of small amplitude, the inputs u_α, u_h are of large amplitude $O(1/\epsilon)$ because they are proportional to the accelerations. A remedy can be achieved by decoupling the high-amplitude part (proportional to $1/\epsilon$) from the rest of the dynamics, which invokes the nonlinear variation of constants formula (Agrachev & Gamkrelidze 1978; Bullo 2002).

A.2. *The nonlinear variation of constants (VOC) formula*

The nonlinear VOC formula is a useful tool for decoupling vector fields of different magnitudes and/or time scales. In particular, it is instrumental for our analysis when the concerned nonlinear system is subjected to high-amplitude periodic forcing. Consider a nonlinear system subjected to a high-frequency, high-amplitude, periodic forcing in the form

$$\dot{x}(t) = f(x(t)) + \frac{1}{\epsilon} G\left(x(t), \frac{t}{\epsilon}\right), \quad x(0) = x_0. \tag{A3a,b}$$

If the time-varying vector field G is periodic in its second argument t, the system (A3a,b) is not directly amenable to averaging, i.e. is not in the form of (A1), because f and G are not of the same order. The VOC formula allows separation of the system (A3a,b) into two companion systems, each of which is amenable to averaging, perhaps after time

scaling. The VOC formula implies (Agrachev & Gamkrelidze 1978; Bullo 2002; Bullo & Lewis 2004; Taha *et al.* 2015*b*; Hassan & Taha 2019)

$$\left.\begin{aligned}\dot{z}(t) &= F(z(t), t), \quad z(0) = x_0 \\ \dot{x}(t) &= \frac{1}{\epsilon}G(x(t), t), \quad x(0) = z(t),\end{aligned}\right\} \quad (A4)$$

where $F(x(t), t)$ is the pullback of the vector field f along the flow Φ_t^G of the time-varying vector field G. This process makes each of the two systems in (A4) (i.e. the z-dynamics and x-dynamics) directly amenable to the averaging theorem (after time scaling $\tau = \omega t$, $\tau = \omega^2 t$, respectively). However, the pullback vector field F in the VOC formula requires computation of flow maps (i.e. solution of part of the differential equation), which may not be analytically tractable for complex systems. Luckily, using the chronological calculus formulation of Agrachev & Gamkrelidze (1978), Bullo (2002) showed that, for a time-invariant f and time-varying G, the pullback vector field $F(x(t), t)$ can be written explicitly in terms of iterated Lie brackets of f and G as

$$F(x(t), t) = f(x(t)) + \sum_{k=1}^{\infty} \int_0^t \cdots \int_0^{s_{k-1}} \left(ad_{G(x(t), s_k)} \ldots ad_{G(x(t), s_1)} f(x) \right) ds_k \ldots ds_1, \quad (A5)$$

where $ad_G f = [G, f]$.

A.3. *Averaging of high-amplitude periodically forced nonlinear systems*

The unsteady aerodynamic system (5.3) is subject to a high-amplitude, high-frequency periodic forcing; i.e. in the form (A3*a*,*b*). Therefore, applying the VOC formula before averaging is necessary to perform proper averaging analysis of the system. The advantage of the VOC formula is that it makes each of the two systems in (A4) individually amenable to the averaging theorem. That is, we have

$$\left.\begin{aligned}\dot{\bar{z}}(t) &= \frac{1}{T}\int_0^T F(\bar{z}, t)\, dt, \quad \bar{z}(0) = x_0 \\ \dot{\bar{x}}(t) &= \frac{1}{T}\int_0^T \frac{1}{\epsilon}G(\bar{x}, t)\, dt, \quad \bar{x}(0) = \bar{z}(t).\end{aligned}\right\} \quad (A6)$$

Moreover, the time-periodic forcing vector field $(1/\epsilon)G(x, t) = g_\alpha(x)u_\alpha(t) + g_h(x)u_h(t)$ is of zero mean (u_α, u_h are zero-mean harmonic functions). Hence, averaging after applying the VOC implies

$$\bar{x}(t) = \bar{z}(t), \quad \dot{\bar{z}} = \bar{F}(\bar{z}). \quad (A7a,b)$$

Hence, one can obtain the averaged dynamics of the original system (A3*a*,*b*) just by averaging the pullback vector field $F(x(t), t)$. Doing so, Theorem A.1 is extended below to high-frequency, high-amplitude, periodically forced systems in the form of (A3*a*,*b*). Finally, it is interesting to note that the use of the VOC formula before averaging can be traced back to Lagrange in his analysis of the perturbed two-body problem (see Sanders *et al.* 2007, pp. 181–184).

THEOREM A.2 (Theorem A in the manuscript). *Consider a NLTP system subject to a high-frequency, high-amplitude, periodic forcing (A3a,b). Assuming that G is a*

T-periodic, zero-mean vector field and both $\boldsymbol{f}$, $\boldsymbol{G}$ are continuously differentiable, the averaged dynamical system corresponding to the system ([A3a,b](#)) is written as

$$\dot{\bar{\boldsymbol{x}}}(t) = \bar{\boldsymbol{F}}(\bar{\boldsymbol{x}}(t)), \tag{A8}$$

where $\bar{\boldsymbol{F}}(\bar{\boldsymbol{x}}(t)) = (1/T) \int_0^T \boldsymbol{F}(\boldsymbol{x}(t), \tau)\, d\tau$, and $\boldsymbol{F}$ is the pullback of $\boldsymbol{f}$ along the flow $\Phi_t^{\boldsymbol{G}}$ of the time-varying vector field $\boldsymbol{G}$ as given in ([A5](#)). Moreover

(i) *If $\bar{\boldsymbol{x}}(0) = \boldsymbol{x}(0)$, then there exist $\sigma > 0$ and $\epsilon^* > 0$ such that $\boldsymbol{x}(t) - \bar{\boldsymbol{x}}(t) = O(\epsilon)\ \forall t \in [0, \sigma/\epsilon]$ and $\forall \epsilon \in [0,\epsilon^*]$.*

(ii) *If $\boldsymbol{x}^*$ is an exponentially stable equilibrium point of ([A8](#)) and if $\|\boldsymbol{x}(0) - \boldsymbol{x}^*\| < r$ for some $r > 0$, then $\boldsymbol{x}(t) - \bar{\boldsymbol{x}}(t) = O(\epsilon)\ \forall t > 0$ and $\forall \epsilon \in [0,\epsilon^*]$. Moreover, there exists an $\epsilon_1 > 0$ such that $\forall \epsilon \in [0,\epsilon_1]$, the system ([A3a,b](#)) has a unique, ϵT-periodic, locally asymptotically stable trajectory that takes values in an open ball of radius $O(1)$ centred at $\boldsymbol{x}^*$.*

The main difference between [Theorem A.1](#) (direct averaging) and [Theorem A.2](#) (VOC and averaging) is that the former guarantees a periodic orbit that is $O(\epsilon)$ around the corresponding fixed point of the averaged dynamics, while the latter allows for larger variations $O(1)$ from the fixed point. Therefore, the application of the VOC formula is essential in analysing the unsteady aerodynamics of a pitching–plunging wing near stall where larger variations from the mean are encountered. It should be emphasized that [Theorem A.1](#) is not a viable option in this case as direct averaging would yield trivial results when applied to the system ([5.3](#)); i.e. it would neglect the entire effects of the pitching–plunging oscillations (represented by the vector field $\boldsymbol{G}$) on the averaged dynamics.

REFERENCES

ABRAHAM, I., DE LA TORRE, G. & MURPHEY, T.D. 2017 Model-based control using koopman operators. arXiv:1709.01568.

ADCL 2019*a* Stabilization of an inverted pendulum under high-frequency excitation (kapitza pendulum). https://www.youtube.com/watch?v=GgYABmG_bto, accessed: 07-11-2017.

ADCL 2019*b* Stabilization of an inverted pendulum under high-frequency excitation (kapitza pendulum). https://www.youtube.com/watch?v=Tnv186IFovQ, accessed: 03-17-2021.

AGRACHEV, A.A. & GAMKRELIDZE, R.V. 1978 The exponential representation of flows and the chronological calculus. *Math. Sbornik* **149** (4), 467–532.

ALBEN, S. & SHELLEY, M. 2005 Coherent locomotion as an attracting state for a free flapping body. *Proc. Natl Acad. Sci. USA* **102** (32), 11163–11166.

ANDRO, J.-Y. & JACQUIN, L. 2009 Frequency effects on the aerodynamic mechanisms of a heaving airfoil in a forward flight configuration. *Aerosp. Sci. Technol.* **13** (1), 71–80.

ANSARI, S.A., ŻBIKOWSKI, R. & KNOWLES, K. 2006 Non-linear unsteady aerodynamic model for insect-like flapping wings in the hover. Part 1: methodology and analysis. *Proc. Inst. Mech. Engrs* **220** (2), 61–83.

ARNOLD, V.I. 1966*a* On an a priori estimate in the theory of hydrodynamical stability. *Izu. Vyssh. Uchebn. Zaued. Matematika* **54** (5), 3–5.

ARNOLD, V.I. 1966*b* Sur la géométrie différentielle des groupes de lie de dimension infinie et ses applications à l'hydrodynamique des fluides parfaits. In *Annales de l'institut Fourier*, vol. 16, pp. 319–361.

ARNOLD, V.I. 1969 Hamiltonian nature of the euler equations in the dynamics of a rigid body and of an ideal fluid. In *Vladimir I. Arnold-Collected Works* (ed. A.B. Givental, B. Khesin, A.N. Varchenko, V.A. Vassiliev & O.Y. Viro), pp. 175–178. Springer.

ARNOL'D, V.I. 2013 *Mathematical Methods of Classical Mechanics*, vol. 60. Springer Science & Business Media.

BAIK, Y.S., BERNAL, L.P., GRANLUND, K. & OL, M.V. 2012 Unsteady force generation and vortex dynamics of pitching and plunging aerofoils. *J. Fluid Mech.* **709**, 37–68.

BAILLIEUL, J. & LEHMAN, B. 1996 Open-loop control using oscillatory inputs. In *CRC Control Handbook* (ed. W.S. Levine), pp. 967–980.

BLOCH, A.M., HOLM, D.D., CROUCH, P.E. & MARSDEN, J.E. 2000 An optimal control formulation for inviscid incompressible ideal fluid flow. In *Proceedings of the 39th IEEE Conference on Decision and Control (Cat. No. 00CH37187)*, vol. 2, pp. 1273–1278. IEEE.

BORISOV, A.V., MAMAEV, I.S. & RAMODANOV, S.M. 2003 Motion of a circular cylinder and n point vortices in a perfect fluid. *Regular Chaotic Dyn.* **8** (4), 449–462.

BORISOV, A.V., MAMAEV, I.S. & RAMODANOV, S.M. 2007 Dynamic interaction of point vortices and a two-dimensional cylinder. *J. Maths Phys.* **48** (6), 065403.

BROCKETT, R.W. 1972 System theory on group manifolds and coset spaces. *SIAM J. Control* **10** (2), 265–284.

BROCKETT, R.W. 1976 Nonlinear systems and differential geometry. *Proc. IEEE* **64** (1), 61–72.

BROCKETT, R.W. 1978 Feedback invariants for nonlinear systems. *IFAC Proc. Volumes* **11** (1), 1115–1120.

BROCKETT, R.W. 1982 Control theory and singular Riemannian geometry. In *New Directions in Applied Mathematics* (ed. P.J. Hilton & G.S. Young), pp. 11–27. Springer.

BROCKETT, R.W. 1983 Asymptotic stability and feedback stabilization. In *Differential Geometric Control Theory 27.1*, pp. 181–191.

BRUNTON, S.L., BRUNTON, B.W., PROCTOR, J.L. & KUTZ, J.N. 2016a Koopman invariant subspaces and finite linear representations of nonlinear dynamical systems for control. *PLoS One* **11** (2), e0150171.

BRUNTON, S.L., PROCTOR, J.L. & KUTZ, J.N. 2016b Discovering governing equations from data by sparse identification of nonlinear dynamical systems. *Proc. Natl Acad. Sci. USA* **113** (15), 3932–3937.

BULLO, F. 2002 Averaging and vibrational control of mechanical systems. *SIAM J. Control Optim.* **41** (2), 542–562.

BULLO, F. & LEWIS, A.D. 2004 *Geometric Control of Mechanical Systems*. Springer.

BUZHARDT, J., FEDONYUK, V. & TALLAPRAGADA, P. 2018 Pairwise controllability and motion primitives for micro-rotors in a bounded stokes flow. *Intl J. Intell. Robot. Appl.* **2** (4), 454–461.

CARR, L.W. 1988 Progress in analysis and prediction of dynamic stall. *J. Aircraft* **25** (1), 6–17.

CHIEREGHIN, N., CLEAVER, D.J. & GURSUL, I. 2019 Unsteady lift and moment of a periodically plunging airfoil. *AIAA J.* **57** (1), 208–222.

CHOI, J., COLONIUS, T. & WILLIAMS, D.R. 2015 Surging and plunging oscillations of an airfoil at low Reynolds number. *J. Fluid Mech.* **763**, 237–253.

CLEAVER, D.J., WANG, Z. & GURSUL, I. 2012 Bifurcating flows of plunging aerofoils at high Strouhal numbers. *J. Fluid Mech.* **708**, 349–376.

CLEAVER, D.J., WANG, Z. & GURSUL, I. 2013 Investigation of high-lift mechanisms for a flat-plate airfoil undergoing small-amplitude plunging oscillations. *AIAA J.* **51** (4), 968–980.

CLEAVER, D.J., WANG, Z., GURSUL, I. & VISBAL, M.R. 2011 Lift enhancement by means of small-amplitude airfoil oscillations at low Reynolds numbers. *AIAA J.* **49** (9), 2018–2033.

CROUCH, P.E. 1984 Spacecraft attitude control and stabilization: applications of geometric control theory to rigid body models. *IEEE Trans. Autom. Control* **29** (4), 321–331.

DICKINSON, M.H., LEHMANN, F.-O. & SANE, S.P. 1999 Wing rotation and the aerodynamic basis of insect flight. *Science* **284** (5422), 1954–1960.

DICKSON, W.B. & DICKINSON, M.H. 2004 The effect of advance ratio on the aerodynamics of revolving wings. *J. Expl Biol.* **207**, 4269–4281.

DRITSCHEL, D.G. & BOATTO, S. 2015 The motion of point vortices on closed surfaces. *Proc. R. Soc. Lond.* A **471** (2176), 20140890.

DUGAS, R. 1988 *A History of Mechanics, Translated into English by JR Maddox*. Dover.

EKATERINARIS, J.A. & PLATZER, M.F. 1998 Computational prediction of airfoil dynamic stall. *Prog. Aerosp. Sci.* **33** (11–12), 759–846.

ELLINGTON, C.P., VAN DEN BERG, C., WILLMOTT, A.P. & THOMAS, A.L.R. 1996 Leading-edge vortices in insect flight. *Nature* **384**, 626–630.

FAIRCHILD, M.J., HASSING, P.M., KELLY, S.D., PUJARI, P. & TALLAPRAGADA, P. 2011 Single-input planar navigation via proportional heading control exploiting nonholonomic mechanics or vortex shedding. In *ASME 2011 Dynamic Systems and Control Conference and Bath/ASME Symposium on Fluid Power and Motion Control*, pp. 345–352. American Society of Mechanical Engineers Digital Collection.

FENERCIOGLU, I. & CETINER, O. 2014 Effect of unequal flapping frequencies on flow structures. *Aerosp. Sci. Technol.* **35**, 39–53.

FLIESS, M., LAMNABHI, M. & LAMNABHI-LAGARRIGUE, F. 1983 An algebraic approach to nonlinear functional expansions. *IEEE Trans. Circuits Syst.* **30** (8), 554–570.

GARRICK, I.E. 1937 Propulsion of a flapping and oscillating airfoil. *NACA Tech. Rep.* NACA-TR-567. National Advisory Committee for Aeronautics.

GARRICK, I.E. 1938 On some reciprocal relations in the theory of nonstationary flows. *NACA Tech. Rep.* 629. National Advisory Committee for Aeronautics.

GOMAN, M. & KHRABROV, A. 1994 State-space representation of aerodynamic characteristics of an aircraft at high angles of attack. *J. Aircraft* **31** (5), 1109–1115.

GUPTA, R. & ANSELL, P.J. 2019 Unsteady flow physics of airfoil dynamic stall. *AIAA J.* **57** (1), 165–175.

GURSUL, I., CLEAVER, D.J. & WANG, Z. 2014 Control of low Reynolds number flows by means of fluid–structure interactions. *Prog. Aerosp. Sci.* **64**, 17–55.

HASSAN, A.M. & TAHA, H.E. 2017 Geometric control formulation and nonlinear controllability of airplane flight dynamics. *Nonlinear Dyn.* **88** (4), 2651–2669.

HASSAN, A.M. & TAHA, H.E. 2019 Differential-geometric-control formulation of flapping flight multi-body dynamics. *J. Nonlinear Sci.* **29**, 1379–1417.

HASSAN, A.M. & TAHA, H.E. 2021 Design of a nonlinear roll mechanism for airplanes using lie brackets for high alpha operation. *IEEE Trans. Aerosp. Electron. Syst.* **57** (1), 462–475.

HEMATI, M.S., ELDREDGE, J.D. & SPEYER, J.L. 2014 Improving vortex models via optimal control theory. *J. Fluids Struct.* **49**, 91–111.

HERMANN, R. 1962 The differential geometry of foliations. II. *J. Math. Mech.* **11**, 303–315.

HERMANN, R. 1963 On the accessibility problem in control theory. In *International Symposium on Nonlinear Differential Equations and Nonlinear Mechanics*, pp. 325–332. Elsevier.

HOLM, D.D., MARSDEN, J.E. & RATIU, T.S. 1998 The Euler–Poincaré equations and semidirect products with applications to continuum theories. *Adv. Math.* **137** (1), 1–81.

HUANG, B. & VAIDYA, U. 2018 Data-driven approximation of transfer operators: naturally structured dynamic mode decomposition. In *2018 Annual American Control Conference (ACC)*, pp. 5659–5664. IEEE.

HUSSEIN, A.A., TAHA, H., RAGAB, S. & HAJJ, M.R. 2018 A variational approach for the dynamics of unsteady point vortices. *Aerosp. Sci. Technol.* **78**, 559–568.

ISIDORI, A. 1995 *Nonlinear Control Systems*, vol. 1. Springer Science & Business Media.

JAKUBCZYK, B. & RESPONDEK, W. 1980 On linearization of control systems. *Bull. Acad. Pol. Sci. Ser. Sci. Math.* **28** (9–10), 517–522.

JONES, M.A. 2003 The separated flow of an inviscid fluid around a moving flat plate. *J. Fluid Mech.* **496**, 405–441.

JONES, R.T. 1938 Operational treatment of the nonuniform lift theory to airplane dynamics. *NACA Tech. Rep.* 667. National Advisory Committee for Aeronautics.

JONES, W.P. 1945 Aerodynamic forces on wings in non-uniform motion. *Tech. Rep.* 2117. British Aeronautical Research Council.

JUANG, J.-N. & PAPPA, R.S. 1985 An eigensystem realization algorithm for modal parameter identification and model reduction. *J. Guid. Control Dyn.* **8** (5), 620–627.

KAMBE, T. 2009 *Geometrical Theory of Dynamical Systems and Fluid Flows*, vol. 23. World Scientific.

KANSO, E., MARSDEN, J.E., ROWLEY, C.W. & MELLI-HUBER, J.B. 2005 Locomotion of articulated bodies in a perfect fluid. *J. Nonlinear Sci.* **15** (4), 255–289.

KARNIADAKIS, G.E. & TRIANTAFYLLOU, G.S. 1989 Frequency selection and asymptotic states in laminar wakes. *J. Fluid Mech.* **199**, 441–469.

KELLY, S.D. & HUKKERI, R.B. 2006 Mechanics, dynamics, and control of a single-input aquatic vehicle with variable coefficient of lift. *IEEE Trans. Robot.* **22** (6), 1254–1264.

KELLY, S.D. & MURRAY, R.M. 2000 Modelling efficient pisciform swimming for control. *Intl J. Robust Nonlinear Control* **10** (4), 217–241.

KELLY, S.D., PUJARI, P. & XIONG, H. 2012 Geometric mechanics, dynamics, and control of fishlike swimming in a planar ideal fluid. In *Natural Locomotion in Fluids and on Surfaces*, pp. 101–116. Springer.

KELLY, S.D. & XIONG, H. 2010 Self-propulsion of a free hydrofoil with localized discrete vortex shedding: analytical modeling and simulation. *Theor. Comput. Fluid Dyn.* **24** (1–4), 45–50.

KHALIL, H.K. 2002 *Noninear Systems*. Prentice-Hall.

KÜSSNER, H.G. 1929 Schwingungen von flugzeugflügeln. In *Jahrbuch der deutscher Versuchsanstalt für Luftfahrt especially Section E3 Einfluss der Baustoff-Dämpfung*, pp. 319–320.

KWATNY, H.G., DONGMO, J.-E.T., CHANG, B.-C., BAJPAI, G., YASAR, M. & BELCASTRO, C. 2012 Nonlinear analysis of aircraft loss of control. *J. Guid. Control Dyn.* **36** (1), 149–162.

LEE, T. & GERONTAKOS, P. 2004 Investigation of flow over an oscillating airfoil. *J. Fluid Mech.* **512**, 313–341.

LEISHMAN, J.G. & BEDDOES, T.S. 1989 A semi-empirical model for dynamic stall. *J. Am. Helicopter Soc.* **34** (3), 3–17.

LEISHMAN, J.G. & CROUSE, G.L. 1989 *State-Space Model for Unsteady Airfoil Behavior and Dynamic Stall*, pp. 1372–1383. AIAA.

LEISHMAN, J.G. & NGUYEN, K.Q. 1990 State-space representation of unsteady airfoil behavior. *AIAA J.* **28** (5), 836–844.

LEONARD, N.E. & KRISHNAPRASAD, P.S. 1995 Motion control of drift-free, left-invariant systems on Lie groups. *IEEE Trans. Autom. Control* **40** (9), 1539–1554.

LESIEUR, M., MÉTAIS, O. & COMTE, P. 2005 *Large-Eddy Simulations of Turbulence*. Cambridge University Press.

LI, J. & WU, Z.-N. 2015 Unsteady lift for the wagner problem in the presence of additional leading/trailing edge vortices. *J. Fluid Mech.* **769**, 182–217.

LIEU, B.K., MOARREF, R. & JOVANOVIĆ, M.R. 2010 Controlling the onset of turbulence by streamwise travelling waves. Part 2. Direct numerical simulation. *J. Fluid Mech.* **663**, 100–119.

LIGHTHILL, J. 1975 Aerodynamic aspects of animal flight. In *Swimming and Flying in Nature*, pp. 423–491. Springer.

LIU, W. 1997*a* An approximation algorithm for nonholonomic systems. *SIAM J. Control Optim.* **35** (4), 1328–1365.

LIU, W. 1997*b* Averaging theorems for highly oscillatory differential equations and iterated Lie brackets. *SIAM J. Control Optim.* **35** (6), 1989–2020.

LOEWY, R.G. 1957 A two-dimensional approximation to unsteady aerodynamics in rotary wings. *J. Aeronaut. Sci.* **24**, 81–92.

LUMLEY, J.L. 2007 *Stochastic Tools in Turbulence*. Courier Corporation.

MAGGIA, M., EISA, S. & TAHA, H. 2019 On higher-order averaging of time-periodic systems: reconciliation of two averaging techniques. *Nonlinear Dyn.* **99**, 813–836.

MARSDEN, J. & WEINSTEIN, A. 1983 Coadjoint orbits, vortices, and clebsch variables for incompressible fluids. *Physica* D **7** (1), 305–323.

MARSDEN, J.E. 1997 Geometric foundations of motion and control. In *Motion, Control, and Geometry: Proceedings of a Symposium, Board on Mathematical Science, National Research Council Education, Washington DC*, pp. 3–19. National Academies Press.

MARSDEN, J.E., O'REILLY, O.M., WICKLIN, F.J. & ZOMBROS, B.W. 1991 Symmetry, stability, geometric phases, and mechanical integrators. *Nonlinear Sci. Today* **1** (1), 4–11.

MCCROSKEY, W.J., MCALISTER, K.W., CARR, L.W. & PUCCI, S.L. 1982 An experimental study of dynamic stall on advanced airfoil section. Volume 1: summary of the experiment. *NACA Tech. Mem.* 84245.

MEERKOV, S.M. 1980 Principle of vibrational control: theory and applications. *IEEE Trans. Autom. Control* **25** (4), 755–762.

MENTER, F.R. 1994 Two-equation eddy-viscosity turbulence models for engineering applications. *AIAA J.* **32** (8), 1598–1605.

MINOTTI, F.O. 2002 Unsteady two-dimensional theory of a flapping wing. *Phys. Rev.* E **66** (5), 051907.

MIR, I., TAHA, H., EISA, S. & MAQSOOD, A. 2018 *A Controllability Perspective of Dynamic Soaring*, vol. 94, pp. 2347–2362. Springer.

MOARREF, R. & JOVANOVIĆ, M.R. 2010 Controlling the onset of turbulence by streamwise travelling waves. Part 1. Receptivity analysis. *J. Fluid Mech.* **663**, 70–99.

MOARREF, R. & JOVANOVIĆ, M.R. 2012 Model-based design of transverse wall oscillations for turbulent drag reduction. *J. Fluid Mech.* **707**, 205–240.

MORGANSEN, K.A., DUIDAM, V., MASON, R.J., BURDICK, J.W. & MURRAY, R.M. 2001 Nonlinear control methods for planar carangiform robot fish locomotion. In *Proceedings 2001 ICRA. IEEE International Conference on Robotics and Automation, 2001*, vol. 1, pp. 427–434. IEEE.

MORGANSEN, K.A., VELA, P.A. & BURDICK, J.W. 2002 Trajectory stabilization for a planar carangiform robot fish. In *Proceedings ICRA'02. IEEE International Conference on Robotics and Automation, 2002*, vol. 1, pp. 756–762. IEEE.

MURRAY, R.M., LI, Z. & SASTRY, S.S. 1994 *A Mathematical Introduction to Robotic Manipulation*. CRC.

MURRAY, R.M. & SASTRY, S.S. 1993 Nonholonomic motion planning: steering using sinusoids. *IEEE Trans. Autom. Control* **38** (5), 700–716.

NARSIPUR, S., HOSANGADI, P., GOPALARATHNAM, A. & EDWARDS, J.R. 2016 Variation of leading-edge suction at stall for steady and unsteady airfoil motions. In *54th AIAA Aerospace Sciences Meeting*, p. 1354.

NAYFEH, A.H. 1973 *Perturbation Methods*. John Wiley and Sons, Inc.

NAYFEH, A.H. & BALACHANDRAN, B. 2004 *Applied Nonlinear Dynamics*. WILEY-VCH Verlag GmbH & Co. KGaA.

NAYFEH, A.H. & MOOK, D.T. 1979 *Nonlinear Oscillations*. John Wiley and Sons, Inc.

NIJMEIJER, H. & VAN DER SCHAFT, A. 1990 *Nonlinear Dynamical Control Systems*. Springer.

OGATA, K. & YANG, Y. 1970 Modern control engineering. Prentice Hall.

PANAH, A.E. & BUCHHOLZ, J.H.J. 2014 Parameter dependence of vortex interactions on a two-dimensional plunging plate. *Exp. Fluids* **55** (3), 1687.

PETERS, D.A. 2008 Two-dimensional incompressible unsteady airfoil theory—an overview. *J. Fluids Struct.* **24**, 295–312.

PETERS, D.A., KARUNAMOORTHY, S. & CAO, W. 1995 Finite-state induced flow models, Part I: two-dimensional thin airfoil. *J. Aircraft* **44**, 1–28.

PLA OLEA, L. 2019 Geometric control theoretic formulation applied to the analysis of pitching and plunging airfoils. Master's thesis, UC Irvine.

POLHAMUS, E.C. 1966 A concept of the vortex lift of sharp-edge delta wings based on a leading-edge-suction analogy. *NASA Tech. Rep.* NASA TN D-3767.

POLLARD, B., FEDONYUK, V. & TALLAPRAGADA, P. 2019 Swimming on limit cycles with nonholonomic constraints. *Nonlinear. Dyn.* **97** (4), 2453–2468.

POPE, S.B. 2000 *Turbulent Flows*. Cambridge University Press.

PULLIN, D.I. & WANG, Z. 2004 Unsteady forces on an accelerating plate and application to hovering insect flight. *J. Fluid Mech.* **509**, 1–21.

RAMESH, K. 2020 On the leading-edge suction and stagnation-point location in unsteady flows past thin aerofoils. *J. Fluid Mech.* **886**, A13.

RAMESH, K., GOPALARATHNAM, A., GRANLUND, K., OL, M.V. & EDWARDS, J.R. 2014 Discrete-vortex method with novel shedding criterion for unsteady aerofoil flows with intermittent leading-edge vortex shedding. *J. Fluid Mech.* **751**, 500–538.

RAVEH, D.E. 2001 Reduced-order models for nonlinear unsteady aerodynamics. *AIAA J.* **39** (8), 1417–1429.

RIVAL, D. & TROPEA, C. 2010 Characteristics of pitching and plunging airfoils under dynamic-stall conditions. *J. Aircraft* **47** (1), 80–86.

RIVAL, D.E., KRIEGSEIS, J., SCHAUB, P., WIDMANN, A. & TROPEA, C. 2014 Characteristic length scales for vortex detachment on plunging profiles with varying leading-edge geometry. *Exp. Fluids* **55** (1), 1660.

ROWLEY, C.W. 2005 Model reduction for fluids, using balanced proper orthogonal decomposition. *Intl J. Bifurcation Chaos* **15** (03), 997–1013.

ROWLEY, C.W., MEZIĆ, I., BAGHERI, S., SCHLATTER, P. & HENNINGSON, D.S. 2009 Spectral analysis of nonlinear flows. *J. Fluid Mech.* **641**, 115–127.

ROZHDESTVENSKY, K.V. & RYZHOV, V.A. 2003 Aerohydrodynamics of flapping-wing propulsors. *Prog. Aerosp. Sci.* **39** (8), 585–633.

SANDERS, J.A., VERHULST, F. & MURDOCK, J.A. 2007 *Averaging Methods in Nonlinear Dynamical Systems*, vol. 2. Springer.

SARYCHEV, A. 2001 Stability criteria for time-periodic systems via high-order averaging techniques. In *Nonlinear Control in the Year 2000* (ed. Alberto Isidori *et al.*), Lecture Notes in Control and Information Sciences, vol. 2, pp. 365–377. Springer.

SASSANO, M. & ASTOLFI, A. 2016 Approximate dynamic tracking and feedback linearization. In *2016 IEEE 55th Conference on Decision and Control (CDC)*, pp. 5688–5693. IEEE.

SASTRY, S. 1999 *Nonlinear Systems: Analysis, Stability, and Control*, vol. 10. Springer.

SCHLICHTING, H., GERSTEN, K., KRAUSE, E., OERTEL, H. & MAYES, K. 1960 *Boundary-Layer Theory*, vol. 7. Springer.

SCHLICHTING, H. & TRUCKENBRODT, E. 1979 *Aerodynamics of the Airplane*. McGraw-Hill.

SCHMID, P.J. 2010 Dynamic mode decomposition of numerical and experimental data. *J. Fluid Mech.* **656**, 5–28.

SCHWARZ, L. 1940 *Brechnung der druckverteilung einer harmonisch sich verformenden tragflache in ebener stromung*, vol. 17. Luftfahrtforsch.

SEARS, W.R. 1956 Some recent developments in airfoil theory. *J. Aeronaut. Sci.* **23** (5), 490–499.

SEARS, W.R. 1941 Some aspects of non-stationary airfoil theory and its practical application. *J. Aeronaut. Sci.* **8** (3), 104–108.

SEDOV, L.I. 1980 Two-dimensional problems of hydrodynamics and aerodynamics. *Moscow Izdatel Nauka* **1**.

SHASHIKANTH, B.N. 2005 Poisson brackets for the dynamically interacting system of a 2d rigid cylinder and n point vortices: the case of arbitrary smooth cylinder shapes. *Regular Chaotic Dyn.* **10** (1), 1–14.

SHASHIKANTH, B.N., MARSDEN, J.E., BURDICK, J.W. & KELLY, S.D. 2002 The hamiltonian structure of a two-dimensional rigid circular cylinder interacting dynamically with *n* point vortices. *Phys. Fluids (1994-present)* **14** (3), 1214–1227.

SHASHIKANTH, B.N., SHESHMANI, A., KELLY, S.D. & MARSDEN, J.E. 2008 Hamiltonian structure for a neutrally buoyant rigid body interacting with n vortex rings of arbitrary shape: the case of arbitrary smooth body shape. *Theor. Comput. Fluid Dyn.* **22** (1), 37–64.

SHASHIKANTH, B.N., SHESHMANI, A., KELLY, S.D. & WEI, M. 2010 Hamiltonian structure and dynamics of a neutrally buoyant rigid sphere interacting with thin vortex rings. *J. Math. Fluid Mech.* **12** (3), 335–353.

SILVA, W.A. 1993 Application of nonlinear systems theory to transonic unsteady aerodynamic responses. *J. Aircraft* **30** (5), 660–668.

SIROVICH, L. 1987 Turbulence and the dynamics of coherent structures. I. Coherent structures. *Q. Appl. Maths* **45** (3), 561–571.

SUSSMANN, H.J. 1973 Orbits of families of vector fields and integrability of distributions. *Trans. Am. Math. Soc.* **180**, 171–188.

SUSSMANN, H.J. 1987 A general theorem on local controllability. *SIAM J. Control Optim.* **25** (1), 158–194.

SUSSMANN, H.J. & JURDJEVIC, V. 1972 Controllability of nonlinear systems. *J. Differ. Equ.* **12** (1), 95–116.

TAHA, H. 2018 Can flapping propulsion boost airplane technology? The flapping-tail concept airplane. *AIAA Paper* 2018-0547.

TAHA, H., HAJJ, M.R. & BERAN, P.S. 2014 State space representation of the unsteady aerodynamics of flapping flight. *Aerosp. Sci. Technol.* **34**, 1–11.

TAHA, H., KIANI, M., HEDRICK, T.L. & GREETER, J.S.M. 2020 Vibrational control: a hidden stabilization mechanism in insect flight. *Sci. Robot.* **5** (46), eabb1502.

TAHA, H. & REZAEI, A.S. 2020 On the high-frequency response of unsteady lift and circulation: a dynamical systems perspective. *J. Fluids Struct.* **93**, 102868.

TAHA, H., TAHMASIAN, S., WOOLSEY, C.A., NAYFEH, A.H. & HAJJ, M.R. 2015a The need for higher-order averaging in the stability analysis of hovering mavs/insects. *Bioinspir. Biomim.* **10** (1), 016002.

TAHA, H., WOOLSEY, C.A. & HAJJ, M.R. 2015b Geometric control approach to longitudinal stability of flapping flight. *J. Guid. Control Dyn.* **39** (2), 214–226.

TAHA, H.E. & HASSAN, A.M. 2021 Nonlinear flight physics of the Lie-bracket roll mechanism. *AIAA Paper* 2021-0252.

TAHMASIAN, S. & WOOLSEY, C.A. 2017 Flight control of biomimetic air vehicles using vibrational control and averaging. *J. Nonlinear Sci.* **27** (4), 1193–1214.

TALLAPRAGADA, P. & KELLY, S.D. 2013 Reduced-order modeling of propulsive vortex shedding from a free pitching hydrofoil with an internal rotor. In *American Control Conference (ACC), 2013*, pp. 615–620. IEEE.

TALLAPRAGADA, P. & KELLY, S.D. 2017 Integrability of velocity constraints modeling vortex shedding in ideal fluids. *J. Comput. Nonlinear Dyn.* **12** (2), 021008.

THEODORSEN, T. 1935 General theory of aerodynamic instability and the mechanism of flutter. *NACA Tech. Rep.* 496. National Advisory Committee for Aeronautics.

USHERWOOD, J.R. & ELLINGTON, C.P. 2002 The aerodynamics of revolving wings. I. Model hawkmoth wings. *J. Expl Biol.* **205**, 1547–1564.

VANDENBERGHE, N., ZHANG, J. & CHILDRESS, S. 2004 Symmetry breaking leads to forward flapping flight. *J. Fluid Mech.* **506**, 147–155.

VELA, P.A. 2003 Averaging and control of nonlinear systems (with application to biomimetic locomotion). PhD thesis, California Institute of Technology.

VELA, P.A., MORGANSEN, K.A. & BURDICK, J.W. 2002 Underwater locomotion from oscillatory shape deformations. In *Proceedings of the IEEE Conference on Decision and Control, Las Vegas, NV*, vol. 2, pp. 2074–2080.

VEPA, R. 1976 On the use of pade approximants to represent unsteady aerodynamic loads for arbitrarily small motions of wings. *AIAA Paper* 1976-17.

VON KÁRMÁN, T. & SEARS, W.R. 1938 Airfoil theory for non-uniform motion. *J. Aeronaut. Sci.* **5** (10), 379–390.

WAGNER, H. 1925 Uber die entstehung des dynamischen auftriebs von tragflugeln. *Z. Angew. Math. Mech.* **5**, 17–35.

WALSH, G.C. & SASTRY, S.S. 1995 On reorienting linked rigid bodies using internal motions. *IEEE Trans. Robot. Automat.* **11** (1), 139–146.

WANG, C. & ELDREDGE, J.D. 2013 Low-order phenomenological modeling of leading-edge vortex formation. *Theor. Comput. Fluid Dyn.* **27** (5), 577–598.

WANG, Z.J., BIRCH, J.M. & DICKINSON, M.H. 2004 Unsteady forces in hovering flight: computation vs experiments. *J. Expl Biol.* **207**, 449–460.

WEBB, C., DONG, H. & OL, M. 2008 Effects of unequal pitch and plunge airfoil motion frequency on aerodynamic response. *AIAA Paper* 2021-1830.

WILCOX, D.C. 2008 Formulation of the kw turbulence model revisited. *AIAA J.* **46** (11), 2823–2838.

WILCOX, D.C. 1998 *Turbulence Modeling for CFD*, vol. 2. DCW industries La Canada.

WILLIAMS, M.O., KEVREKIDIS, I.G. & ROWLEY, C.W. 2015 A data–driven approximation of the Koopman operator: extending dynamic mode decomposition. *J. Nonlinear Sci.* **25** (6), 1307–1346.

WOOLSEY, C.A. & LEONARD, N.E. 2002 Stabilizing underwater vehicle motion using internal rotors. *Automatica* **38** (12), 2053–2062.

XIAO, Q. & LIAO, W. 2010 Computational study of oscillating hydrofoil with different plunging/pitching frequency. *J. Aero Aqua Biomech.* **1** (1), 64–70.

YAN, Z., TAHA, H. & HAJJ, M.R. 2014 Geometrically-exact unsteady model for airfoils undergoing large amplitude maneuvers. *Aerosp. Sci. Technol.* **39**, 293–306.

YONGLIANG, Y., BINGGANG, T. & HUIYANG, M. 2003 An analytic approach to theoretical modeling of highly unsteady viscous flow excited by wing flapping in small insects. *Acta Mechanica Sin.* **19** (6), 508–516.

YOUNG, J. & LAI, J.C. 2007 Vortex lock-in phenomenon in the wake of a plunging airfoil. *AIAA J.* **45** (2), 485–490.